

Response to reviewers

Submission bg-2019-15 to *Biogeosciences*

Editor

Dear Marijke et al.,

I have now received two reports on your contribution. Both find your manuscript suitable for publication in BG following (minor) revisions. Please follow their detailed comments closely in revising your ms.

Sincerely,

Markus

We thank the editor for the positive assessment of our manuscript. We have revised the manuscript and below we provide point-to-point answers to the comments of the reviewers: when applicable, we indicated where adjustments were made in the text (note: when we refer to line numbers in which we have made adjustments, we refer to the line numbering of the revised manuscript with “track changes”/All Markup). The reviewers’ comments are in regular font; our replies are in bold font.

Sincerely, also on behalf of all co-authors,

Marijke de Bar

Response to referee #1

Review: This manuscript investigates long-chain diols (LCDs) in sediment trap time series from five tropical sites (tropical North Atlantic, Cariaco Basin, Mozambique Channel) to assess seasonal variations in fluxes of LCDs and associated proxies (Long chain Diol Index and Diol Index). These data are compared with other lipid proxies (alkenones and GDGTs) and previous published data (primary production, SST,..). Results show that surface sediment LDI temperatures in the Atlantic and Mozambique Channel compare well with the average LDI-derived temperatures from the overlying sediment traps, as well as with decadal annual mean SST. In the Mozambique Channel and the tropical Atlantic, the LDI temperatures reveal minimal seasonal change although there are clear seasonal SST contrasts, which is likely due to lateral advection of re-suspended sediment. In the Cariaco Basin, a strong seasonality in the LDI is observed, which is linked to the upwelling season and stratification of the water column. In addition, in the Atlantic, the Diol Index reflects a pre-upwelling signal, whereas in the Cariaco Basin, the Diol Index seems to be an indicator of upwelling intensity. This paper is a valuable contribution to the understanding of the seasonal production of LCDs in marine environments and how it is translated in the temperature proxy LDI and the Diol Index (upwelling proxy). A strength of the paper is that the LCD data has been compared with other available data for each site (primary production, SST, alkenones, GDGTs,...), which gives a broader picture and supports the interpretations based on LCDs. The writing style is clear and precise and the interpretations are generally supported by the data. This manuscript is thus suitable for *Biogeosciences*. However, the current manuscript could be improved before publication. Please find my comments below.

We thank the referee for the positive assessment and for the comments, which we will discuss below.

General comments:

Diol index and upwelling: The authors argue that, in the Cariaco Basin, the Diol Index is an excellent indicator of upwelling intensity (Lines 476-480). However, when looking at the 1999-2000 time series, high values of the diol index actually occur when the primary production decreases. What are the R2 values (and p values) that justify “a strong correlation with primary production rates”?

We agree with the reviewer that for the 1999-2000 time series there is a disagreement during January/February when the diol index increases and primary production rates decrease. We now mention this in the revised version of the manuscript. The ‘strong correlation’ between the diol index and primary production is based purely on the visual agreement between both time series. We were not able to perform a correlation analysis since the data are differently spaced in time. We have also emphasized this in the revised version manuscript (lines 493-496):

“In the Cariaco Basin, the Diol Index shows a strong correlation (visually as correlation analysis was not possible due to differently spaced data in time) with primary production rates, suggesting that *Proboscia* productivity was synchronous with total productivity (Fig. 8), although for the 1999-2000 time series there is a disagreement during January/February.”

In addition, for the eastern Atlantic (M1 trap), the authors argue that the Diol Index reflects a preupwelling signal, consistent with the current knowledge on *Proboscia* ecology (Lines 509-526). I would like to see more discussion that explains why at one location the Diol index indicates preupwelling conditions, whereas it seems to be an indicator of upwelling intensity at another location.

We agree that this seems contradictory and requires more discussion, which we have implemented in the revised version of the manuscript. The Diol Index is an upwelling indicator based on the assumption that *Proboscia* diatoms generally thrive in upwelling regions. However, the index is in fact an indicator for *Proboscia* productivity, and whether it reflects upwelling/pre-upwelling/stratification/etc. conditions will depend on the region and the local ecological dynamics determining the role of *Proboscia* diatoms (e.g., Rampen et al., 2014; de Bar et al., 2018). Studies have shown that *Proboscia* diatoms are often more dominant during early/pre-upwelling because they need relatively little silica and they are able to migrate to deeper waters to obtain nutrients (Koning et al., 2001) and sediment trap data from Wakeham et al. (2002), Prahl et al. (2000), Sinninghe Damsté et al. (2003) and Rampen et al. (2007) show that *Proboscia* lipids (diols and/or hydroxyl methyl alkanates) are highest during early upwelling. Therefore, we hypothesize that this Diol Index maximum during spring which we observe for station M1 in the Atlantic might be a pre/early-upwelling signal since the upwelling in the Guinea Dome often occurs between July and October (Siedler et al., 1992). Indeed, *Proboscia* diatoms do not reflect early-upwelling in every region. Reports of *Proboscia* spp. blooms vary from stratification to early-upwelling to postbloom, and from high nutrients to low nutrients (see Rampen et al., 2014; references in Table 1). Apparently, in the Cariaco Basin, *Proboscia* diatoms bloom relatively synchronous with general productivity, as evidenced from the agreement between the Diol Index and primary production time series, emphasizing the value of sediment trap studies like ours in revealing regional differences in proxy signals. We have added the following lines (546-549):

“Our results clearly show that the Diol Index reflects different things in different regions. This is due to the ecology of *Proboscia* spp. where blooms occur during stratification to early upwelling to postbloom, and from high nutrients to low nutrients (see Rampen et al., 2014; references in Table 1). Therefore, the type of conditions reflected by the Diol Index is specific for every region.”

Keto-ols as oxidation products (Lines 578-586): An alternative explanation for the non-detection of 1,14-keto-ols would be that keto-ols are not oxidation products of LCDs, but rather produced by unknown organism(s) (Versteegh et al., 1997). Previous studies have indeed shown the absence of

evidence of conversion of diols into their corresponding oxidized keto-ols (Jiang et al., 1994; Méjanelle et al. 2003; Shimokawara et al., 2010). I think the authors should acknowledge this.

We agree, and we have mentioned this hypothesis as well (lines 611-615):

*“Alternatively, the keto-ols are not oxidation products but are produced by unknown organisms in the water column. In fact, Méjanelle et al. (2003) observed trace amounts of C₃₀ 1,13- and C₃₂ 1,15-keto-ols in cultures of the marine eustigmatophyte *Nannochloropsis gaditana*. Thus, an alternative explanation for the non-detection of 1,14-keto-ols is that in contrast to the 1,15-keto-ols, they were not produced in the water column.”*

Figures: I think the current order of the figures does not necessarily follow the logic of the results/discussion. For more clarity, I would suggest modifying the order as follows: Fig. 2 should be Fig. 8; Fig. 3 should be Fig. 2; Fig. 8 should be Fig. 8; Fig. 4 should be Fig. 3; Fig. 5 should be Fig. 8; Fig. 6 should be Fig. 4; Fig. 8 should be Fig. 5; Fig. 8 should be Fig. 6.

We have re-ordered as follows:

Fig. 2 → Fig. 2

Fig. 3 → Fig. 3

Fig. 4 → Fig. 9

Fig. 5 → Fig. 4

Fig. 6 → Fig. 5

Fig. 7 → Fig. 6

Fig. 8 → Fig. 7

Fig. 9 → Fig. 8

Specific comments:

Line 25: specify “with emphasis on the temperature proxy Long Chain Diol Index”.

We have corrected this accordingly.

Line 27: specify “similar to the two other lipid-based temperature proxies TEX86 and UK’37”.

We have corrected this accordingly.

Line 27: “In addition” instead of “However”.

We have corrected this accordingly.

Line 29: Could be rephrased as: “In contrast, the LDI in the Cariaco Basin shows larger seasonal variation”.

We have corrected this accordingly.

Line 48: Need references.

We have added the review of Tierney (2014) as reference.

Lines 48-50: Could be rephrased as: “However, research showed that despite their highest abundance being recorded in the upper 100 m of the water column, Thaumarchaeota can be present down to 5000 m depth (Karner et al., 2001; Herndl et al., 2005)”.

We have corrected this accordingly.

Line 69: “for autumn to summer” should be “for autumn and summer”.

We have corrected this accordingly.

Figure 1: indicate in the caption what NEC, NECC, SEC, MC, GD, NBC and GC stand for. Is it possible to add the position of the ITCZ during the boreal winter?

We have clarified the abbreviations in the figure caption and indicated the position of the ITCZ during boreal winter.

Line 200: What are CTD measurements?

We refer here to temperature measurements of seawater at 1m water depth sampled by CTD. We have clarified this.

Line 256-258: Could diols be found in the DCM:MeOH (1:1; v/v) fraction? Have you checked?

We thank the reviewer for noticing this, since the sentence is incorrect: not the MeOH fractions were analyzed for diols, but the DCM:MeOH (1:1, v/v) fractions. We have corrected this.

Line 369: Should be as: “C28 and C30 1,13- (0–3 %), the C30 1,15- (44–99 %), and the C32 1,15-diols (0–7%)”.

We have corrected this accordingly.

Lines 367-376: I think a table showing the presence/absence for each diols (and the % of total LCDs) at the different traps (M1, M2,...) and different sites (Atlantic, Mozambique Channel, Cariaco Basin) would be useful to clearly see which diols are detected for each location. The Figure 2 is used to discuss the preservation between traps and sediments rather than showing the diols detected.

We do not fully agree, since the number of figures is already extensive, as is the result section, and we consider this relatively detailed.

Line 392: Fig. 4 is cited before Fig. 8. I think the order of the figures should be changed (see previous comment).

We have changed the order of figures, see comment above.

Line 397: cite Figure 7.

We have corrected this.

Response to referee #2

General comments

In this study, de Bar et al. presented long-chain diol (LCD) data from five sites; three along a longitudinal transect in the tropical Atlantic, the Cariaco Basin and the Mozambique Channel. LCD derived indices, i.e. Long-chain Diol Index (LDI) and Diol Index, are used to reconstruct past SST and upwelling, respectively. These proxies are relatively new compared to those based on alkenones and GDGTs, thus have not been as well studied. This is where this study comes in. de Bar et al analyzed LCDs from sediment traps and underlying sediments. For the sites where alkenones and GDGT data do not yet exist, the authors also analyzed these biomarkers in addition to LCDs C1 to allow multi-proxy comparison for all the sites. The well-designed experiment thus allows the authors to investigate various aspects of the LCDs and their associated proxies, including the temporal evolution (seasons to years), settling processes, as well as comparison with other commonly applied biomarker proxies. The data presented by de Bar et al. generally show that LDI-derived temperatures agree within error with instrumental data in the Atlantic, albeit with different amplitude of change. At upwelling sites, the Diol Index seems to either record a pre-upwelling signal or show the same trend as in primary productivity.

The study fits the scope of Biogeosciences, and will also be of interest to readers from other community such as paleoclimate. The manuscript is generally well-written and accessible. I do, however, feel that some figures could be further improved for clarity. I find the "Results" section too long and some discussion unclear or not fully supported by the data, especially in section 4.3. Below are suggestions and comments that I hope will help the authors in further improving the manuscript. Once the concerns are addressed, I strongly recommend the publication of this manuscript.

We thank the referee for the positive assessment and for the comments, which we will discuss below.

Specific comments

#Line 34-36: Clunky sentence. Please rephrase.

We have rephrased as follows (lines 35-39):

“Lastly, we observed large seasonal variations in the Diol Index, as indicator of upwelling conditions, at three sites: in the Eastern Atlantic potentially linked to Guinea Dome upwelling, in the Cariaco Basin likely caused by seasonal upwelling, and in the Mozambique Channel where underlying mechanisms are indefinable but where Diol Index variations may be driven by upwelling from favorable winds and/or eddy migration.”

#Line 43: "Conte 2006" should be "Conte et al 2006"

We have corrected this.

#Line 96-97: "ITCZ migrates southward during boreal winter" - would be useful to have this marked in Figure 1 too.

We have indicated the approximate position of the ITCZ during boreal winter in Figure 1.

#Line 100: Insert abbreviation (SEC) after South Equatorial Current.

We have inserted this abbreviation.

#Line 116: replace "/" with either a space or comma.

We have replaced it with a comma.

#Line 119: "as result" should be "as a result"

We have corrected this accordingly.

#Line 125: "latitudinal transect" is a transect across latitudes. What you have is a "longitudinal transect", i.e. with sites spanning longitudes at a fixed latitude (~12°N). C2

Thank you for this correction, we have corrected this throughout the manuscript.

#Line 183-184: Varved sediments have annual resolution. Since you mentioned "annually to decadal resolved climate records", do you mean "laminated sediments" instead?

Yes, we have corrected this accordingly.

#Line 224: "weight sub-aliquots" is confusing. Suggested rephrasing "sub-aliquots (by weight)".

We have corrected this accordingly.

#Line 237-238: Confusing sentence. Sounds like you analyzed both ketone and GDGT fractions by both GC and GC/MS - which is likely not the case. Please rephrase.

We have rephrased as follows (lines 244-247):

“The ketone fraction was also dissolved in ethyl acetate, and analyzed by GC and GC/MS. The GDGT fraction was dissolved in hexane:isopropanol (99:1, v/v), filtered through a 0.45 μm polytetrafluoroethylene (PTFE) filter and analyzed by HPLC-MS.”

#Line 285-287: Technically this is a variant of the original BIT index proposed by Hopmans et al 2004. Please rephrase the paragraph to reflect this.

We have rephrased as follows (lines 293-296):

“The Branched Isoprenoid Tetraether (BIT) index is a proxy for the relative contribution of terrestrial derived organic carbon (Hopmans et al., 2004). We have calculated the modified version as reported by de Jonge et al. (2014; 2015) which is based on the original index as proposed by Hopmans et al. (2004), but includes the 6-methyl brGDGTs.”

#Line 296: This is not the first time GC is mentioned in the manuscript. Spell out "gas chromatograph" at the first mention instead of here. Also, there is no need to define the abbreviation at each mention.

We have corrected this accordingly.

#Line 308-309: Tierney and Tingley (2018) is not the first to notice the warm-end limit of UK³⁷, i.e. an issue which has been in debate since the 90s. Please include the original references.

We have rephrased as follows (lines 316-321):

“We have also applied the recently proposed BAYSPLINE Bayesian calibration of Tierney and Tingley (2018). They and others have shown that the U^K₃₇ estimates substantially attenuate above temperatures of 24 °C (e.g., Conte et al., 1998; Goñi et al., 2001; Sicre et al., 2002). The Bayesian calibration moves the upper limit of the U^K₃₇ calibration from approximately 28 to 29.6 °C at unity. Since our traps are located in tropical regions with SSTs > 24 °C, we have applied this calibration as well.”

#Line 313: "gas chromatograph (GC)" see comment to Line 296.

We have corrected this accordingly.

#Line 314: "mass spectrometer (MS)" see comment to Line 296.

We have corrected this accordingly.

#Section 2.5 Time-series analysis: Since the result of the time-series analysis is not a main part of the results and discussion, I would suggest to either (A) remove this rather long section or (b) move it to the supplement and add a supplementary figure depicting the result (which is briefly discussed in the text but not shown).

We agree, and we have moved these methods to the supplements.

#Section 3. Results: I had a hard time going through the 4-page long results section. Given the large data set spanning several sites and including several biomarkers and their associated proxies (for which I applaud the authors), this is perhaps inevitable. But I think that it will make the section more accessible for the reader if the authors could reduce the text by 10 to 20%, either by restructuring the text, tabulating some of the results and/or limiting the result description to only the main findings that are discussed in the following section.

We agree that the results section is a bit on the long side, and we have removed a few sentences.

#Line 362: "longitudinal" not "latitudinal".

We have corrected this.

#Line 368-369: Confusing. Rephrase please.

We have rephrased as follows (lines 378-380):

“The LCDs detected in the sediment trap samples and surface sediments from the tropical North Atlantic (Fig. 2) are the C₂₈, C₃₀ and C_{30:1} 1,14-, C₂₈ and C₃₀ 1,13-, the C₃₀ 1,15-, and C₃₂ 1,15-diols.”

#Line 430-431: "during January and July" - replace with "between January and July". Also, it is not clear at all in Fig 5d that the TEX₈₆H temperatures are lower during these months. Please rephrase.

We have rephrased accordingly, and we agree that for M4 this decrease in TEX₈₆^H temperatures is not clearly visible and we have removed this statement.

#Line 444: I'd argue that there's some structural similarity between the Diol Index and chlorophyll-a records.

We do not believe this (visual) agreement is strong enough to make a statement about this. Therefore, we would like to refrain from discussing this.

#Line 482: What are "15 and 18°"? Latitude?

We have added the latitude.

#Line 491-497: I strongly urge the authors to at least show the wavelet analysis in the supplementary info to support their claim. Please also mark the cool water events in Figure 8b to support the claim that ". . .the timing of the observed time periods of enhanced Diol Index variability are similar to those of the cool water events. . ."

We now show the wavelet analysis in the supplements. However, we cannot mark the cool water events in Fig 8b since we do not know the timings of these events for this specific time interval. We merely wanted to emphasize that Malauene et al. (2014) reported bimonthly frequency and a boreal winter timing for these cold events, which we also observe in our wavelet analysis. Below are the wavelet results which we have included in the supplements:

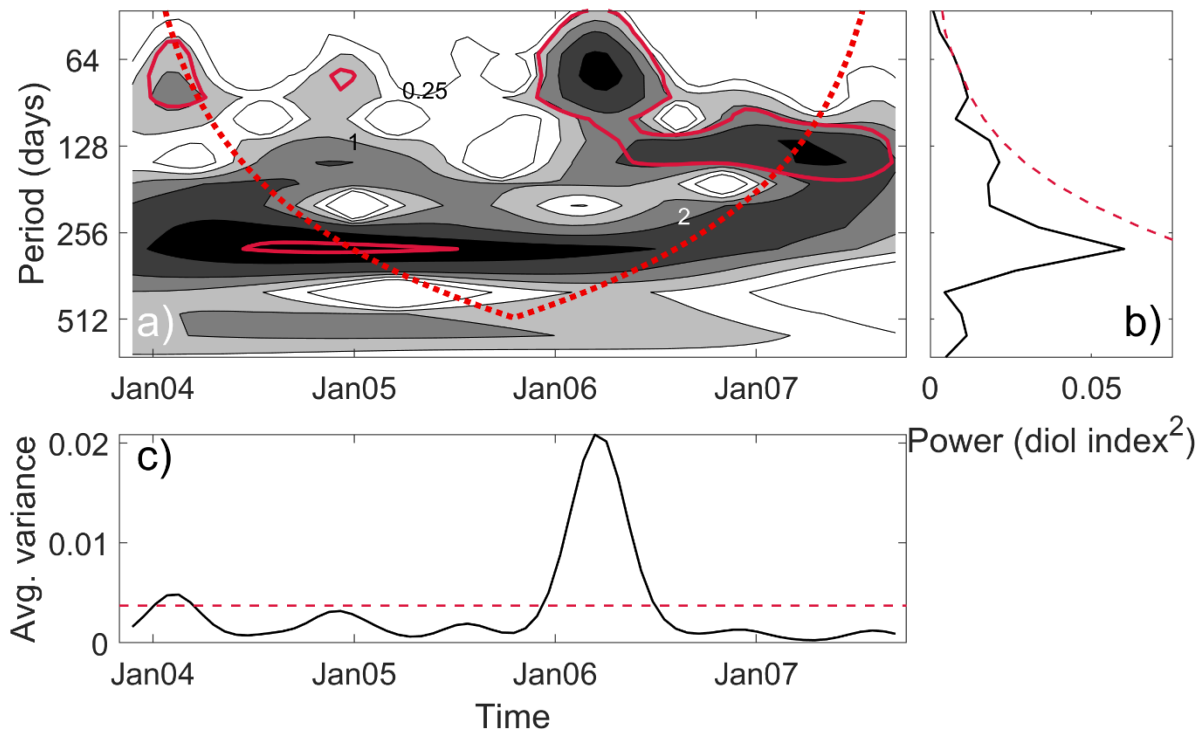


Fig. S1. a) The local wavelet power spectrum of the Diol Index in the sediment traps of the Mozambique Channel using the Morlet wavelet, normalized by the standard deviation. On the x-axis is time, and the y-axis shows the Fourier period in days. The shaded contours are at normalized variances of 0.25, 0.5, 1, 2, and 4. The bold red contour encloses regions of greater than 95% confidence for a red-noise process with a lag-1 coefficient of 0.72. Regions below the dotted red curve are where edge effects become important (Torrence and Compo, 1998). b) Global wavelet spectrum of Diol Index – the wavelet spectrum averaged in time over the whole time series. The red dashed line is the 95% confidence level. c) Wavelet power averaged over the range of scales from 42 to 90 days. The black line is the time series of the average variance within the 42-90-day range. The red dashed line is the 95% confidence level.

#Line 496-497: I am not following this. Assuming a sampling interval of 21 days - that would give us about 21 data points per year. With so few data points in the time series, it would be impossible to detect 4 cycles in the first half of 2006. Please clarify.

With a sampling interval of 21 days, the highest frequency we can detect is half the sampling rate, i.e. 1/42 cycles per day (or 8.7 cycles per year). As we describe on line 508-511, and now show in figure S1, the wavelet analysis showed significant variability at about bimonthly frequency (60-day period) during some parts of the time series, most notably the first half of 2006. We have rephrased the sentence on line 516-517 to: “The strongest variability of the Diol Index at about bimonthly frequencies occurred in the first half of 2006.”

#Line 498-499: It would be helpful to mark the timing of the passage of eddies in Fig 8b.

This is a good suggestion; however, it is not completely straightforward to do this in a thorough way. We first need to decide on a definition of a passing eddy – there are several possibilities, for example using the instrumental records of temperature, salinity, or current velocity at the

moorings (one useful criterion could be, for example, lateral velocity shear between the eastern and western side), or an independent record such as dynamic height derived from satellite altimetry. Because of this uncertainty we refrain from indicating this.

#Line 504: "Fig 5c" shows LDI not Diol Index.

We have corrected this.

#Line 508: "Fig 5e" shows LDI not Diol Index.

We have corrected this.

#Line 522: Change "due its closer vicinity" to "due to its closer vicinity"

We have corrected this accordingly.

#Line 523: "NW Africa" This is mentioned only once in the text. Spell out NW.

We have corrected this accordingly.

#Line 556: r (and p) values are more appropriate as a metric to describe the correlation between two variables than r^2 (which is used to describe how well the data fit the linear regression model).

We now mention the r and p values here.

#Line 570-571: Explain briefly why one can expect LCD and levoglucosan to have similar response to degradation, e.g. in terms of their chemical behavior/structure.

We have included the following (lines 594-596):

“Both are functionalized polar lipids with alcohol groups and thus are chemically relatively similar when compared to e.g. fatty acids (carboxyl group) or n-alkanes (no functional groups).”

#Line 578: "for" or "in" the Atlantic?

We have corrected this sentence.

#Line 583-586: Include in the sentence the producers of 1,13- and 1,15-diols.

We have corrected this accordingly.

#Line 614: Replace "minimal differences" with "minimal variations/variability".

We have corrected this accordingly.

#Line 625-627: It is true for LDI and UK'37 that the difference between proxy temperatures and instrumental SST increase during the warmer months, but not for TEX86H. The difference between TEX86H and SST for the cooler months are almost as large as that during the warmer months, and these differences are within the calibration error. Please rephrase the sentence to reflect this.

We have added the following (lines 655-657):

“Interestingly, the $U^{K'_{37}}$ - and TEX^H_{86} -derived temperature trends show the same phenomenon (Turich et al., 2013; Fig. 8), where the proxy temperatures are cooler than the measured temperatures during the warmer months. However, in contrast to the $U^{K'_{37}}$ and LDI, the TEX^H_{86} also overestimates SST overestimation during the cold months.”

#Line 638-640: Taken into account proxy uncertainty, I do not think it is possible to discern if the LDI temperatures are closer to SST or 20m (some temperatures are even higher than SST!), as the isotherms of the upper 30m are so close to each other anyway during the upwelling season. In any case, a habitat depth of the upper 20m is consistent with previous studies as well (as mentioned in line 646 - 649). Please rephrase the sentence.

We agree, and we have now emphasized that the temperature differences are within calibration error (lines 669-673):

“During upwelling, LDI-temperatures agree better with SST, implying that the habitat of the LCD producers potentially was closer to the surface, coincident with the shoaling of the nutricline and thermocline (Fig. 10). However, these absolute differences in LDI-temperatures are generally within the calibration error (2 °C), and these seasonal variations in LDI-temperatures should thus be interpreted with caution.”

#Line 676-690: This discussion is not supported by the < 2 °C of temperature difference between TEX86H and satellite-SST that is well within the calibration error of TEX86H. In fact, the difference is even smaller than that between the LDI temperature and satellite SST in the North Atlantic (Fig 5), which the authors did not discuss since the differences are mostly within the calibration error. The authors also need to justify why they compared the 0-150m (instead of from the same water depths as the calibration) temperatures with the temperature estimates calculated using the 0-200m calibration. Since the focus of the paper is on LCD proxies, and this subsurface TEX86 finding was not mentioned in the abstract nor the conclusions, I would suggest to remove this paragraph.

We agree with the referee that this discussion is outside the scope of this manuscript, and that indeed we are discussing temperature differences which are within calibration error. We therefore have removed this part of the discussion.

#Line 700-703: See comment on #Line 638-640.

We have rephrased as follows (lines 732-736):

“In the Cariaco Basin we observe a seasonal signal in the LDI linked to the upwelling season reflecting temperatures of the upper ca. 30 m of the water column.”

#Fig. 2: It took me a while to understand this figure. I think stacked bar chart would make a better option here, so instead of 12 panels with 3 bars each, you'd have 12 stacked bars which give you the same amount of information.

We have tried this option, but to our opinion this did not improve clarity as it visually suggests that the preservation percentages are summed. We therefore chose to use our original figure.

#Line 1184: Change "concentration" to "concentrations".

We have corrected this accordingly.

#Line 1185: Change "than" to "then".

We have corrected this accordingly.

#Fig. 3: It is impossible to tell which lines/variables correspond to which y-axes without going through the caption. I would suggest to change the color of the right y-axis and its label (Total mass flux) to grey, i.e. the same color as the plot for the variable.

We agree, and we have adjusted the figure accordingly.

#Fig. 8: This figure is mentioned for the first time at line 5XX in the section "Discussion" - I suggest to renumber it according to the order of its appearance in the text.

We have re-ordered the figures, also on suggestion of referee#1.

#Fig. 6: Specify at least in the caption if the annual mean WOA SST is averaged over latitudes or at a fixed latitude. I would also remove the panel on the left and the annual mean T0-150m in panel d if line 676-690 are removed.

The annual mean WOA SSTs are specific for the coordinates of the surface sediments; we have now emphasized this in the caption.

Since we have removed the discussion part on the subsurface TEX_{86} , we have also removed the left panel (a) and the annual mean T_0 - $T_{150\text{m}}$ and TEX_{86} -subsurface temperatures in panel d.

Additional comment:

We have replaced Fig. 9 since we by accident previously plotted the summed 1,13-/1,15-diol concentrations instead of the summed flux-weighted 1,13-/1,15-diol concentrations.

1 **Long chain diols in settling particles in tropical oceans:**
2 **insights into sources, seasonality and proxies.**

3

4 Marijke W. de Bar^{*,1}, Jenny E. Ullgren², Robert C. Thunnell[‡], Stuart G. Wakeham³, Geert-Jan
5 A. Brummer^{4,5}, Jan-Berend W. Stuut^{4,5}, Jaap S. Sinninghe Damsté^{1,6} and Stefan Schouten^{1,6}

6

7 ¹ NIOZ Royal Netherlands Institute for Sea Research, Department of Marine Microbiology
8 and Biogeochemistry, and Utrecht University, P.O. Box 59, 1790 AB Den Burg, Texel, the
9 Netherlands

10 ² Runde Miljøsentor, Runde, Norway

11 ³ Skidaway Institute of Oceanography, University of Georgia, 10 Ocean Science Circle,
12 Savannah, USA

13 ⁴ NIOZ Royal Netherlands Institute for Sea Research, Department of Ocean Systems, and
14 Utrecht University, P.O. Box 59, 1790 AB Den Burg, Texel, the Netherlands

15 ⁵ Vrije Universiteit Amsterdam, Faculty of Science, Department of Earth Sciences, De
16 Boelelaan 1085, 1081HV Amsterdam, the Netherlands

17 ⁶ Department of Earth Sciences, Faculty of Geosciences, Utrecht University, the Netherlands

18

19 * Corresponding author: Marijke W. de Bar (Marijke.de.Bar@nioz.nl)

20

21

[‡] Deceased: 30 July 2018.

22 ABSTRACT

23 In this study we have analyzed sediment trap time series from five tropical sites to assess seasonal
24 variations in concentrations and fluxes of long-chain diols (LCDs) and associated proxies with emphasis
25 on the Long chain Diol Index (LDI) temperature proxy. For the tropical Atlantic, we observe that
26 generally less than 2 % of LCDs settling from the water column are preserved in the sediment. The
27 Atlantic and Mozambique Channel traps reveal minimal seasonal variations in the LDI, similar to the
28 two other lipid-based temperature proxies TEX₈₆ and U^{K'}₃₇. ~~However~~In addition, annual mean LDI-
29 derived temperatures are in good agreement with the annual mean satellite-derived sea surface
30 temperatures (SSTs). In contrast, the Cariaco Basin the LDI in the Cariaco Basin shows larger seasonal
31 variation, as do the TEX₈₆ and U^{K'}₃₇. Here, the LDI underestimates SST during the warmest months,
32 which is ~~likely~~ possibly due to summer stratification and the habitat depth of the diol producers
33 deepening to around 20 to 30 m. Surface sediment LDI temperatures in the Atlantic and Mozambique
34 Channel compare well with the average LDI-derived temperatures from the overlying sediment traps,
35 as well as with decadal annual mean SST. Lastly, we observed large seasonal variations in the Diol
36 Index, as indicator of upwelling conditions, at three sites, in the Eastern Atlantic potentially linked to
37 Guinea Dome upwelling ~~(Eastern Atlantic)~~, in the Cariaco Basin likely caused by seasonal upwelling,
38 ~~(Cariaco Basin)~~ and in the Mozambique Channel where Diol Index variations may be driven by
39 upwelling from favorable winds and/or eddy migration. seasonal upwelling and/or eddy migration
40 ~~(Mozambique Channel).~~

42 1. Introduction

43 Several proxies exist for the reconstruction of past sea surface temperature (SST) based on lipids. The
44 $U^{K'}_{37}$ is one of the most applied proxies and is based on the unsaturation of long-chain alkenones (LCAs),
45 which are produced by phototrophic haptophyte algae, mainly the cosmopolitan *Emiliania huxleyi*
46 (Volkman et al., 1980; Brassell et al., 1986; Prahl and Wakeham, 1987; Conte et al., 1994). This index
47 exhibits a strong positive correlation with SST (Müller et al., 1998; Conte [et al.](#), 2006). Another widely
48 used organic paleotemperature proxy is the TEX_{86} , as originally proposed by Schouten et al. (2002),
49 based on the relative distribution of archaeal membrane lipids, i.e. glycerol dialkyl glycerol tetraethers
50 (GDGTs), and in the marine realm are mainly thought to be derived from the phylum Thaumarchaeota.
51 Schouten et al. (2002) showed that the TEX_{86} index measured in marine surface sediments is correlated
52 with SST, and since then its application in paleoenvironmental studies has increased ([see e.g. review by](#)
53 [Tierney, 2014](#)). However, research showed that despite their highest abundance [being recorded of](#)
54 ~~Thaumarchaeota~~ in the upper 100 m of the water column, ~~they~~ [Thaumarchaeota](#) can be present down to
55 5000 m depth (Karner et al., 2001; Herndl et al., 2005). Accordingly, GDGTs may be found in high
56 concentrations below 100 m depth (e.g., Sinninghe Damsté et al., 2002; Wuchter et al., 2005) and several
57 studies have indicated that TEX_{86} might be more reflective of subsurface temperatures in some regions
58 (e.g., Huguet et al., 2007; Lopes dos Santos et al., 2010; Kim et al., 2012; 2015; Schouten et al., 2013;
59 Chen et al., 2014; Tierney et al., 2017; see Zhang and Liu, 2018 for review).

60 Most recently a SST proxy based on the distribution of long-chain diols (LCDs), called the Long-chain
61 Diol Index, or LDI was proposed (Rampen et al., 2012). This index is a ratio of 1,13- and 1,15-diols
62 (i.e., alcohol groups at position C-1 and C-13 or C-15), and the analysis of globally distributed surface
63 sediments revealed that this index strongly correlates with SST. Since then, the index has been applied
64 in several paleoenvironmental studies (e.g., Naafs et al., 2012; Lopes dos Santos et al., 2013; Jonas et
65 al., 2017; Warnock et al., 2017). However, large gaps still remain in the understanding of this proxy.
66 The largest uncertainty is that the main marine producer of LCDs is unknown. Although these diols have
67 been observed in cultures of certain marine eustigmatophyte algae (e.g. Volkman et al., 1992; 1999;
68 Méjanelle et al., 2003; Rampen et al., 2014b), the LCD distributions in cultures are different from those

69 observed in marine sediments. Furthermore, Balzano et al. (2018) combined lipid analyses with 18S
70 rRNA gene amplicon sequencing on suspended particulate matter (SPM) and did not find a significant
71 direct correlation between LCD concentrations and sequences of known LCD-producers. Rampen et al.
72 (2012) observed the strongest empirical relation between surface sediment derived LDI values and SSTs
73 for autumn ~~to~~ and summer, suggesting that these are the main growth seasons of the source organisms.
74 Moreover, the strongest correlation was also observed for the upper 20 m of the water column,
75 suggesting that the LCDs are likely produced by phototrophic algae which thrive in the euphotic zone.
76 Nevertheless, LDI-temperatures based on surface sediments reflect an integrated signal of many years,
77 which complicates the interpretation of the LDI in terms of seasonal production and depth of export
78 production.

79 One way of resolving seasonality in LCD flux and LDI is to analyze time series samples from sediment
80 traps that continuously collect sinking particles in successive time intervals over periods of a year or
81 more. Such studies have been carried out for the $U^{K'}_{37}$ as well as for the TEX_{86} and associated lipids
82 (e.g., Müller and Fischer, 2001; Wuchter et al., 2006; Huguet et al., 2007; Fallet et al., 2011; Yamamoto
83 et al., 2012; Rosell-Melé and Prahl, 2013; Türich et al., 2013). However, very few studies have been
84 done for LCDs. Villanueva et al. (2014) carried out a sediment trap study in Lake Challa (East Africa)
85 and Rampen et al. (2008) in the upwelling region off Somalia. The latter study showed that 1,14-diols,
86 produced by *Proboscia* diatoms strongly increased early in the upwelling season in contrast to 1,13- and
87 1,15-diols and thus can be used to trace upwelling. However, ~~none~~ neither of these sediment trap studies
88 have evaluated the LDI.

89 In this study, we assess seasonal patterns of the LDI for sediment trap series at five sites, i.e., in the
90 Cariaco Basin, the Mozambique Channel and three sites in the tropical North Atlantic and compared the
91 LDI values to satellite-derived SST, as well as results obtained for other temperature proxies, i.e. the
92 TEX^H_{86} and $U^{K'}_{37}$. Moreover, for the Atlantic and Mozambique Channel, we compare the sediment trap
93 proxy signals with those preserved in the underlying sediments, after settling and burial. Finally, we
94 assess the applicability of the Diol Index, based on 1,14-diols produced by *Proboscia* diatoms
95 (Sinninghe Damsté et al., 2003), as tracer of upwelling and/or productivity in these regions.

96 2. Materials and methods

97 2.1 Study sites and sample collection

98 2.1.1 Tropical North Atlantic

99 The ocean current and wind patterns of the tropical Atlantic are mostly determined by the seasonal
100 latitudinal shift of the intertropical convergence zone (ITCZ; Figure 1). The ITCZ migrates southward
101 during boreal winter, and northward during boreal summer. During summer, the south-east trade winds
102 prevail, whereas during winter the north-east trade winds intensify. The north-east trade winds drive the
103 North Equatorial Current (NEC) which flows westward. South of ~~this current~~ the NEC, ~~flows~~ the North
104 Equatorial Countercurrent (NECC) flows towards the east (Stramma and Schott, 1999). The South
105 Equatorial Current (SEC) flows westward and branches off in the north Brazil Current (NBC; Stramma
106 and Schott, 1999). When the ITCZ is in the north, the NBC retroflects off the South American coast,
107 and is carried eastward into the NECC, and thus into the western tropical Atlantic (e.g., Richardson and
108 Reverdin, 1987). North of the NBC, the Guiana Current (GC) disperses the outflow from the Amazon
109 River towards the Caribbean Sea. (Müller-Karger et al., 1988; 1995). However, during boreal summer
110 the NBC may retroflect, carrying the Amazon River plume far into the western Atlantic (e.g., Lefèvre
111 et al., 1998; Müller-Karger et al., 1998; Coles et al., 2013). In fact, every late summer/autumn, the
112 Amazon River outflow covers around 2×10^6 km² of the western North Atlantic, and the river delivers
113 approximately half of all freshwater input into the tropical Atlantic (see Araujo et al., 2017 and
114 references therein).

115 The eastern tropical North Atlantic is characterized by upwelling caused by the interaction between the
116 trade winds and the movement of the ITCZ. Cropper et al. (2014) measured upwelling intensity along
117 the NW African coastline between 1981 and 2012, in terms of wind speed, SST and other meteorological
118 data. They recognized three latitudinal zones: weak permanent annual upwelling north of 26° N, strong
119 permanent upwelling between 21° and 26° N and seasonal upwelling between 12° and 19° N related to
120 the seasonal migration of the trade winds. Southeast of Cape Verde, large-scale cyclonic circulation
121 forms the Guinea Dome (GD; Fig. 1), which centers around 10° N, 22° W (Mazeika, 1967), i.e., close
122 to mooring site M1. ~~It~~ The GD is a thermal upwelling dome, formed by near-surface flow fields

123 associated with the westward NEC, the eastward NECC and the westward North Equatorial
124 Undercurrent (NEUC) (Siedler et al., 1992). It forms a cyclonic circulation as a result of the eastward
125 flowing NECC and the westward flowing NEC (Rossignol and Meyrueis, 1964; Mazeika, 1967). The
126 GD develops from late spring to late fall due to the northward ITCZ position and the resulting Ekman
127 upwelling, but shows significant interannual variability (Siedler et al., 1992; Yamagata and Iizuka, 1995;
128 Doi et al., 2009) judging from general ocean circulation models. According to Siedler et al. (1992),
129 upwelling is most intense between July and October when the ITCZ is in the GD region and the NECC
130 is strongest.

131 At three sites, we analyzed five sediment trap series along a latitudinal-longitudinal transect in the North
132 Atlantic (~12° N) to determine seasonal variations in the LDI. This transect has been studied previously
133 for Saharan dust deposition in terms of grain sizes (van der Does et al., 2016), as the tropical North
134 Atlantic receives approximately one third of the wind-blown Saharan dust (e.g., Duce et al., 1991; Stuut
135 et al., 2005), which might potentially act as fertilizer because of the high iron levels (e.g., Martin and
136 Fitzwater, 1988; Korte et al., 2017; Guirreiro et al., 2017; Goudie and Middleton, 2001 and references
137 therein). Furthermore, Korte et al. (2017) assessed mass fluxes and mineralogical composition,
138 Guerreiro et al. (2017) measured coccolith fluxes for two of the time series, while Schreuder et al.
139 (2018a; 2018b) measured long-chain *n*-alkanes, long-chain *n*-alkanols and fatty acids, and levoglucosan
140 for the same sediment trap samples and surface sediments as analyzed in this study.

141 At site M1 (12.00° N, 23.00° W), the sediment trap, referred to as M1U, was moored at a water depth
142 of 1150 m (Fig. 1). This mooring is located in the proximity of the Guinea Dome, and might therefore
143 potentially be influenced by seasonal upwelling. At station M2 (13.81° N, 37.82° W), two sediment
144 traps were recovered, i.e., an ‘upper’ (M2U) trap at a water depth of 1235 m, and a ‘lower’ (M2L) trap
145 at a depth of 3490 m. Lastly, at mooring station M4 (12.06° N, 49.19° W), also an upper and lower trap
146 series were recovered and analyzed (M4U and M4L), at 1130 and 3370 m depth, respectively. This
147 mooring site may seasonally be affected by Amazon River discharge (van der Does et al., 2016; Korte
148 et al., 2017; Guirreiro et al., 2017; Schreuder et al., 2018a). All sediment traps were equipped with 24
149 sampling cups, which sampled synchronously over 16-day intervals from October 2012 to November

150 2013, using HgCl₂ as a biocide and borax as a pH buffer to prevent in situ decomposition of the collected
151 material.

152

153 **2.1.2 Mozambique Channel**

154 The Mozambique Channel is located between Madagascar and Mozambique and is part of the Agulhas
155 Current system hugging the coast of South Africa (Lutjeharms, 2006). The Agulhas Current system is
156 an important conveyor in the transport of warm and salty waters from the Indian to the Atlantic Ocean
157 (Gordon, 1986; Weijer et al., 1999; Peeters et al., 2004). The northern part of the channel is also
158 influenced by the East African monsoon winds (Biaostoch and Krauss, 1999; Sætre and da Silva, 1982;
159 Malauene et al., 2014). Between September and March, these winds blow from the northeast, parallel
160 to the Mozambique coastline, favoring coastal upwelling. Additionally, the Mozambique Channel is
161 largely influenced by fast-rotating, mesoscale eddies which migrate southward towards the Agulhas
162 region. Using satellite altimetry, Schouten et al. (2003) observed on average 4 to 6 eddies, ca. 300 km
163 in diameter, propagating yearly from the central Mozambique Channel (15° S) toward the Agulhas area
164 (35° S) between 1995 and 2000. Seasonal upwelling occurs off Northern Mozambique (between ca. 15
165 and 18° S) (Nehring et al., 1987; Malauene et al., 2014), from August to March with a dominant period
166 of about two months although periods of one to four weeks have also been observed (Malauene et al.,
167 2014).

168 The sediment trap was moored at 16.8° S and 40.8° E, at a water depth of 2250 m (Fig. 1; Fallet et al.,
169 2010, 2011) and of the same type as used for the North Atlantic transect. We analyzed the LCD proxies
170 for two respective time intervals: the first interval covers ca. 3.5 years, from November 2003 to
171 September 2007, with a sampling interval of 21 days. The second interval covers another year, between
172 February 2008 and February 2009, with a sampling interval of 17 days. Previously, Fallet et al. (2011)
173 published foraminiferal, U^K₃₇ and TEX₈₆ records for the first time interval, and the organic carbon
174 content for the follow-up time series. For further details on the deployments and sample treatments, we
175 refer to Fallet et al. (2011, 2012). The two surface sediments are located across the narrowest transect

176 between Mozambique and Madagascar, and were analyzed for U^{K}_{37} and TEX_{86} by Fallet et al. (2012)
177 and for LCDs by Lattaud et al. (2017b).

178

179 **2.1.3 Cariaco Basin**

180 The Cariaco Basin is one of the largest marine anoxic basins (Richards, 1975), located on the continental
181 shelf of Venezuela. The basin is characterized by permanent stratification and strongly influenced by
182 the migration of the intertropical convergence zone (ITCZ). During late autumn and winter, the ITCZ
183 migrates to the south which results in decreased precipitation and trade wind intensification which in
184 turn induces upwelling and surface water cooling. This seasonal upwelling is a major source of nutrients
185 that leads to strong phytoplankton growth along the Venezuelan coast (e.g., Müller-Karger et al., 2001;
186 Thunell et al., 2007). Between August and October, the ITCZ moves northward again, resulting in a
187 rainy season and diminishing of the trade winds inhibiting upwelling. During this wet season the
188 contribution of terrestrially derived nutrients is higher. Due to the prevalent anoxic conditions in the
189 basin, there is no bioturbation which has resulted in the accumulation of ~~varved-laminated~~ sediments
190 which provide excellent annually to decadal resolved climate records (e.g., Peterson et al., 1991;
191 Hughen et al., 1996; 1998). Moreover, in November 1995, a time series experiment started to facilitate
192 research on the link between biogeochemistry and the downward flux of particulate material under
193 anoxic and upwelling conditions (Thunell et al., 2000). This project (CARIACO;
194 <http://imars.marine.usf.edu/cariaco>) involved hydrographic cruises (monthly), water column chemistry
195 measurements and sediment trap sampling (every 14 days). One mooring containing four automated
196 sediment traps (Honjo and Doherty, 1988) was deployed at 10.50° N and 64.67° W, at a bottom depth
197 of around 1400 m. These traps were moored at 275 m depth, just above the oxic/anoxic interface (Trap
198 A), 455 m (Trap B), 930 m (Trap C) and 1255 m (Trap D). All traps contain a 13-cup carousel which
199 collected sinking particles over 2 weeks, and were serviced every half year. For further details on trap
200 deployment and recovery, and sample collection, storage and processing we refer to Thunell et al. (2000)
201 and Goñi et al. (2004). In addition to the sediment trap sampling, the primary productivity of the surface
202 waters was measured every month using ^{14}C incubations (Müller-Karger et al., 2001; 2004). For this

203 study, we investigated two periods, i.e., May 1999–May 2000 and July 2002–July 2003 for Traps A and
204 B. These years include upwelling and non-upwelling periods, as well as a disastrous flooding event in
205 December 1999 (Turich et al., 2013). Turich et al. (2013) identified the upwelling periods, linked to the
206 migration of the ITCZ, as indicated by decreasing SST in the CTD (temperature at -1 m water depth)
207 and satellite-based measurements (indicated by grey boxes in figures 9-8 and 10), and shoaling of the
208 average depths of primary production and increased primary production. Moreover, Turich et al. (2013)
209 evaluated the $U^{K_{37}}$ and TEX_{86} proxies for the same two time series for which we analyzed the LCD
210 proxies.

211

212 **2.2 Instrumental data**

213 Satellite SST, precipitation and wind speed time series of the M1, M2 and M4 moorings in the Atlantic
214 derive from Guerreiro et al. (2017 and in revision) who retrieved these data from the Ocean Biology
215 Processing Group (OBPG, 2014) (Frouin et al., 2003), the Goddard Earth Sciences Data and Information
216 Services Center (2016) (Huffman et al., 2007; Xie and Arkin, 1997) and NASA Aquarius project (2015a;
217 2015b) (Lee et al., 2012) (see supplement of Guerreiro et al., 2017 for detailed references). The SST
218 and Chlorophyll *a* time series data for the Mozambique Channel were adapted from Fallet et al. (2011),
219 who retrieved these data from the Giovanni database (for details see Fallet et al., 2011). Surface sediment
220 proxy temperatures were compared to annual mean SST estimates derived from the World Ocean Atlas
221 (2013) (decadal averages from 1955 to 2012; Locarnini et al., 2013). Sea surface temperature data for
222 the Cariaco Basin were adopted from Turich et al. (2013) and combined with additional CTD
223 temperatures from the CARIACO time series data base for the depths of 2, 5, 10, 15 and 20 m
224 (<http://www.imars.usf.edu/CAR/index.html>); CARIACO time series composite CTD profiles; lead
225 principal investigator: Frank Müller-Karger).

226

227 2.3 Lipid extraction

228 2.3.1 Tropical North Atlantic

229 The 120 sediment trap samples were sieved through a 1 mm mesh wet-split into five aliquots (van der
230 Does et al., 2016), of which one was washed with Milli-Q water, freeze-dried and homogenized for
231 chemical analysis (Korte et al., 2017). For organic geochemistry, ~~weight~~ sub-aliquots (by weight) were
232 extracted as described by Schreuder et al. (2018a). Shortly, ca. 100 mg dry weight of sediment trap
233 residue, and between 1.5 and 10 g of dry weight of surface sediment were extracted by ultrasonication
234 using a mixture of dichloromethane:methanol (DCM:MeOH) (2:1; v/v), and dried over a Na₂SO₄
235 column. For quantification of LCDs, LCAs and GDGTs, we added the following internal standards to
236 the total lipid extracts (TLEs): 2.04 µg C₂₂ 7,~~16~~-16-diol (Rodrigo-Gamiz et al., 2015), 1.50 µg 10-
237 nonadecanone (C_{19:0} ketone) and 0.1 µg C₄₆ GDGT (Huguet et al., 2006), respectively. Subsequently,
238 the TLEs were separated into apolar (containing *n*-alkanes), ketone (containing LCAs) and polar
239 (containing LCDs and GDGTs) fractions over an activated (2h at 150 °C) Al₂O₃ column by eluting with
240 hexane/DCM (9:1; v/v), hexane/DCM (1:1; v/v) and DCM/MeOH (1:1; v/v), respectively. The apolar
241 fractions were analyzed by Schreuder et al. (2018a) for *n*-alkanes. Polar fractions were split for GDGT
242 (25 %) and LCD (75 %) analysis. The LCD fraction was silylated by the addition of BSTFA (*N,O*-
243 bis(trimethylsilyl)trifluoroacetamide) and pyridine, and heating at 60 °C for 20 min, after which ethyl
244 acetate was added prior to analysis. The ketone fraction was also dissolved in ethyl acetate, and analyzed
245 by GC and GC/MS. ~~and~~ The GDGT fraction was dissolved in hexane:isopropanol (99:1, v/v), ~~and~~
246 ~~analyzed by GC and GC/MS.~~ ~~Next, the GDGT fractions were~~ filtered through a 0.45 µm
247 polytetrafluoroethylene (PTFE) filter and analyzed by HPLC-MS.

248 2.3.2 Mozambique Channel

249 Aliquots of the sediment trap samples from the Mozambique Channel were previously extracted and
250 analyzed by Fallet et al. (2011) and Fallet et al. (2012), respectively. The sediment trap material was
251 extracted by ultrasonication using a mixture of DCM/MeOH (2:1; v/v), dried over Na₂SO₄, and
252 separated into apolar, ketone and polar fractions via alumina pipette column chromatography, by eluting
253 with hexane/DCM (9:1; v/v), hexane/DCM (1:1; v/v) and DCM/MeOH (1:1; v/v), respectively. These

254 existing polar fractions of the sediment trap material were silylated (as described above), dissolved in
255 ethyl acetate and re-analyzed for LCDs by GC-MS. Since no record was kept of the aliquoting of extracts
256 and polar fractions, we report the results in relative abundance rather than concentrations and fluxes of
257 diols.

258 **2.3.3 Cariaco Basin**

259 Sediment trap material was extracted as described by Turich et al. (2013). Briefly, 1/16 aliquots of the
260 trap samples were extracted by means of Bligh-Dyer extraction with sonication using a phosphate buffer
261 and a trichloroacetic acid (TCA) buffer, after which the extracts were separated by adding 5 % NaCl in
262 solvent-extracted distilled deionized water, and the organic phase was collected and the aqueous phase
263 was extracted two more times. The extracts were pooled and dried over Na₂SO₄ and separated by means
264 of Al₂O₃ column chromatography, eluting with hexane:DCM (9:1; v/v), DCM:MeOH (1:1; v/v) and
265 MeOH. For this study, ~~this latter~~ the DCM:MeOH (1:1; v/v) fraction was silylated (as described above),
266 dissolved in ethyl acetate, and analyzed for LCDs using GC-MS. Similar to the Mozambique Channel
267 samples, no record was kept of the aliquoting of extracts and polar fractions, and thus we report the
268 results in relative abundance.

269

270 **2.4 Instrumental analysis**

271 **2.4.1 GDGTs**

272 The GDGT fractions of the surface sediments and sediment traps SPM samples of the tropical North
273 Atlantic were analyzed for GDGTs by means of Ultra High Performance Liquid Chromatography Mass
274 Spectrometry (UHPLC-MS). We used an Agilent 1260 HPLC, which is equipped with an automatic
275 injector, interfaced with a 6130 Agilent MSD, and HP Chemstation software according to Hopmans et
276 al. (2016). Compound separation was achieved by 2 silica BEH HILIC columns in tandem (150 mm x
277 2.1 mm; 1.7 μm; Waters Acquity) in normal phase, at 25 °C. GDGTs were eluted isocratically for 25
278 min with 18 % B, followed by a linear gradient to 35 % B in 25 minutes and finally a linear gradient to
279 100 % B in the last 30 min. A = hexane; B = hexane:isopropanol (9:1; v/v). The flow rate was constant
280 at 0.2 mL min⁻¹, and the injection volume was 10 μL. The APCI-MS conditions are described by

281 Hopmans et al. (2016). Detection and quantification of GDGTs was achieved in single ion monitoring
282 (SIM) mode of the protonated molecules ($[M+H]^+$) of the GDGTs. We used a mixture of crenarchaeol
283 and the C₄₆ GDGT (internal standard) to assess the relative response factor, which was used for
284 quantification of the GDGTs in the samples (c.f. Huguet et al., 2006).

285 Sea surface temperatures were calculated by means of the TEX₈₆^H as defined by Kim et al. (2010), which
286 is a logarithmic function of the original TEX₈₆ index (Schouten et al., 2002):

$$287 \quad \text{TEX}_{86}^H = \log \frac{[\text{GDGT-2}] + [\text{GDGT-3}] + [\text{Cren}']}{[\text{GDGT-1}] + [\text{GDGT-2}] + [\text{GDGT-3}] + [\text{Cren}']} \quad [1]$$

288 where the numbers indicate the number of cyclopentane moieties of the isoprenoid GDGTs, and *Cren'*
289 reflects an isomer of crenarchaeol, i.e. containing a cyclopentane moiety with a *cis* stereochemistry
290 (Sinninghe Damsté et al., 2018). The TEX₈₆^H values were translated to SSTs using the core-top
291 calibration of Kim et al. (2010):

$$292 \quad \text{SST} = 68.4 \times \text{TEX}_{86}^H + 38.6 \quad [2]$$

293 The Branched Isoprenoid Tetraether (BIT) index is a proxy for the relative contribution of terrestrial
294 derived organic carbon (de Jonge et al., 2014; 2015 Hopmans et al., 2004). We have calculated the
295 modified version as reported by de Jonge et al. (2014; 2015) which ~~This ratio~~ is based on the original
296 index as proposed by Hopmans et al. (2004), but includes the 6-methyl brGDGTs:

$$297 \quad \text{BIT} = \frac{[\text{brGDGT Ia}] + [\text{brGDGT IIa+IIa'}] + [\text{brGDGT IIIa+IIIa'}]}{[\text{brGDGT Ia}] + [\text{brGDGT IIa+IIa'}] + [\text{brGDGT IIIa+IIIa'}] + [\text{Cren}]} \quad [3]$$

298 where the numbers reflect different branched GDGTs (see Hopmans et al., 2004) and *Cren* reflects
299 crenarchaeol. The branched GDGTs were always around the detection limit in the Atlantic samples,
300 implying a BIT index of around zero and thus minimal influence of soil organic carbon (Hopmans et
301 al., 2004), and thus the BIT index is not discussed any further.

302

303 2.4.2 LCAs

304 The ketone fractions of the surface sediments and sediment traps samples of the tropical North Atlantic
305 were analyzed for LCAs on an Agilent 6890N gas chromatograph (GC) with flame ionization
306 detection (FID) after dissolving in ethyl acetate. The GC was equipped with a fused silica column with
307 a length of 50 m, a diameter of 0.32 mm, and a coating of CP Sil-5 (film thickness = 0.12 μm). Helium
308 was used as carrier gas, and the flow mode was a constant pressure of 100 kPa. The ketone fractions
309 were injected on-column at a starting temperature of 70 °C, which increased by 20 °C min⁻¹ to 200 °C
310 followed by 3 °C min⁻¹ until the final temperature of 320 °C was reached. This end temperature was
311 held for 25 min.

312 The $U_{37}^{K'}$ index was calculated according to Prahl and Wakeham (1987):

$$313 \quad U_{37}^{K'} = \frac{[C_{37:2}]}{[C_{37:2}] + [C_{37:3}]} \quad [4]$$

314 The $U_{37}^{K'}$ values were translated to SST after the calibration of Müller et al. (1998):

$$315 \quad SST = \frac{U_{37}^{K'} - 0.044}{0.033} \quad [5]$$

316 We have also applied the recently proposed BAYSPLINE Bayesian calibration of Tierney and Tingley
317 (2018). They and others have shown~~showed~~ that the $U_{37}^{K'}$ estimates substantially attenuate above
318 temperatures of 24 °C (e.g., Conte et al., 1998; Goñi et al., 2001; Sicre et al., 2002). The Bayesian
319 calibration~~, moving moves~~ the upper limit of the $U_{37}^{K'}$ calibration from approximately 28 to 29.6 °C at
320 unity. Since our traps are located in tropical regions with SSTs > 24 °C, we have applied this calibration
321 as well.

322

323 2.4.3 LCDs

324 The silylated polar fractions were injected on-column on an Agilent 7890B ~~gas chromatograph (GC)~~
325 ~~GC~~ coupled to an Agilent 5977A ~~mass spectrometer (MS)~~. The starting temperature was 70 °C, and
326 increased to 130 °C by 20 °C min⁻¹, followed by a linear gradient of 4 °C min⁻¹ to an end temperature of
327 320 °C, which was held for 25 min. 1 μL was injected, and separation was achieved on a fused silica

328 column (25 × 0.32 mm) coated with CP Sil-5 (film thickness 0.12 μm). Helium was used as carrier gas
329 with a constant flow of 2 mL min⁻¹. The MS operated with an ionization energy of 70 eV. Identification
330 of LCDs was done in full scan mode, scanning between *m/z* 50–850, based on characteristic
331 fragmentation patterns (Volkman et al., 1992; Versteegh et al., 1997). Proxy calculations and LCD
332 quantifications were performed by analysis in SIM mode of the characteristic fragments (*m/z* 299, 313,
333 327 and 341; Rampen et al., 2012; *m/z* 187 for internal diol standard). For quantification of LCDs in the
334 sediment traps and seafloor sediments of the tropical Atlantic, the peak areas of the LCDs were corrected
335 for the average relative contribution of the selected SIM fragments to the total ion counts, i.e., 16 % for
336 the saturated LCDs, 9 % for unsaturated LCDs and 25 % for the C₂₂ 7,16-diol internal standard.

337 Sea surface temperatures were calculated using the LDI ~~index~~, according to Rampen et al. (2012):

$$338 \quad \text{LDI} = \frac{[\text{C}_{30} \text{ 1,15-diol}]}{[\text{C}_{28} \text{ 1,13-diol}] + [\text{C}_{30} \text{ 1,13-diol}] + [\text{C}_{30} \text{ 1,15-diol}]} \quad [6]$$

339 These LDI values were converted into SSTs using the following equation (Rampen et al., 2012):

$$340 \quad \text{SST} = \frac{\text{LDI} - 0.095}{0.033} \quad [7]$$

341 Upwelling conditions were reconstructed using the Diol Index as proposed by Rampen et al. (2008):

$$342 \quad \text{Diol Index} = \frac{[\text{C}_{28} \text{ 1,14-diol}] + [\text{C}_{30} \text{ 1,14-diol}]}{[\text{C}_{28} \text{ 1,14-diol}] + [\text{C}_{30} \text{ 1,14-diol}] + [\text{C}_{30} \text{ 1,15-diol}]} \quad [8]$$

343 In 2010, Willmott et al. introduced an alternative Diol Index, which is defined as the ratio of 1,14-diols
344 over 1,13-diols. Since the index of Rampen et al. (2008) includes the C₃₀ 1,15-diol, it can be affected by
345 temperature variation, and therefore we would normally prefer to use the index of Willmott et al. (2010).
346 However, we often did not detect the C₂₈ 1,13-diol, or it co-eluted with cholest-5-en-7-one-3β-ol,
347 compromising the calculation of the Diol Index of Willmott et al. (2010). Moreover, the temperature
348 variations in all three sediment traps are minimal as recorded by the LDI. Accordingly, we chose to
349 apply the Diol Index according to Rampen et al. (2008).

350 Potential fluvial input of organic carbon was determined by the fractional abundance of the C₃₂ 1,15-
351 diol (de Bar et al., 2016; Lattaud et al., 2017a):

352
$$FC_{32\ 1,15\text{-diol}} = \frac{[C_{32\ 1,15\text{-diol}}]}{[C_{28\ 1,13\text{-diol}}] + [C_{30\ 1,13\text{-diol}}] + [C_{30\ 1,15\text{-diol}}] + [C_{32\ 1,15\text{-diol}}]} \quad [9]$$

353 The fractional abundance of the C₃₂ 1,15-diol was always lower than 0.23, suggesting low input of river
354 derived organic carbon (Lattaud et al., 2017a).

355

356 **2.5 Time-series analysis**

357 ~~We performed time series spectral analysis on the Diol Index data from the Mozambique Channel to~~
358 ~~assess the influence of meso-scale eddies. Analyses were performed in MATLAB®. The two parts of~~
359 ~~the Diol Index time series, i.e. the 2003–2007 and the 2008–2009 periods, were analysed both separately~~
360 ~~and together. The data were linearly interpolated in time (to 21-day intervals for the 2003–2007 period,~~
361 ~~and 17-day intervals for the 2008–2009 period) to adjust for disjunct sampling intervals or short gaps,~~
362 ~~and detrended. A runs test for randomness (Gibbons & Chakraborty, 2003) showed that for the second,~~
363 ~~shorter time series (2008–2009) the null hypothesis—that the values in the series are in random order—~~
364 ~~could not be rejected at the 5% significance level. The second series also lacked statistically significant~~
365 ~~autocorrelation according to the Ljung-Box test (Ljung & Box, 1978). Therefore, there was little point~~
366 ~~in analysing the shorter 2008–2009 time series for periodicity. We performed a wavelet analysis to~~
367 ~~detect transient features in the Mozambique Channel Diol Index 2003–2007 time series following the~~
368 ~~methods of Torrence and Compo (1998; <http://paos.colorado.edu/research/wavelets/>) and using the~~
369 ~~Morlet wavelet as mother wavelet.~~

370

371 **3. Results**

372 **3.1 Tropical North Atlantic**

373 We have analyzed sediment trap samples from a latitudinal-longitudinal transect (~ 12°N) in the tropical
374 North Atlantic (two upper traps at ca. 1200 m water depth, and three lower traps at ca. 3500 m; Fig. 1),
375 covering November 2012–November 2013, as well as seven underlying surface sediments, for LCDs,
376 LCAs and GDGTs. Below we present the results for these lipid biomarkers and associated proxies.

377

3.1.1 LCDs

378 The LCDs detected in the sediment trap samples and surface sediments from the tropical North Atlantic
 379 (Fig. 2) are the C_{28} -~~and~~ ~~(mono-unsaturated and saturated)~~ C_{30} and $C_{30:1}$ 1,14- (not in surface sediments)
 380 ~~(between 1 and 49 % of all LCDs)~~, C_{28} and C_{30} 1,13-~~(0–3 %)~~, ~~and~~ the C_{30} 1,15-~~(44–99 %)~~, and C_{32}
 381 1,15-diol_{SS} ~~(0–7 %)~~. ~~In the M2 and M4 traps, the C_{30} 1,15 diol constitutes between 87 and 95 % of total~~
 382 ~~LCDs.~~ We detected the C_{28} 1,14- diol and C_{29} -OH fatty acid in the traps from M1 and M4, in a few
 383 samples of the M2 traps and in all surface sediments. ~~Similarly, the C_{28} 1,14 diol was detected in all~~
 384 ~~samples from M1 and M4, in only a few M2 samples and in all surface sediments.~~ For most samples
 385 from M2U and M2L, the C_{28} 1,14-diol was often part of a high background signal, making identification
 386 and quantification problematic. In these cases, 1,14-diol fluxes and Diol Index were solely based on the
 387 (saturated and mono-unsaturated) C_{30} 1,14-diol. ~~In contrast, the saturated C_{30} 1,14 diol was detected in~~
 388 ~~all samples.~~

389 The average [1,13+1,15]-diol flux is $2.6 (\pm 1.0) \mu\text{g m}^{-2} \text{d}^{-1}$ at M1U, $1.4 (\pm 1.2)$ and $1.2 (\pm 1.1) \mu\text{g m}^{-2} \text{d}^{-1}$
 390 ¹ for M2U and M2L, respectively, and $7.0 (\pm 7.8)$ and $2.2 (\pm 3.3) \mu\text{g m}^{-2} \text{d}^{-1}$ for M4U and M4L,
 391 respectively (Fig. 3). The [1,13+1,15]-diol and 1,14-diol concentrations in the underlying sediments
 392 vary between $0.05 \mu\text{g g}^{-1}$ and $0.50 \mu\text{g g}^{-1}$, and between 3 ng g^{-1} and $0.06 \mu\text{g g}^{-1}$, respectively. ~~The~~
 393 ~~[1,13+1,15]-LCD flux is more than three times higher in the upper trap of M4 than in the lower trap,~~
 394 ~~whereas at M2, where the average LCD fluxes are much lower, the difference is not appreciable.~~ The
 395 1,14-diol flux for M1U averages $0.5 (\pm 0.8) \mu\text{g m}^{-2} \text{d}^{-1}$ with a pronounced maximum of $3.5 \mu\text{g m}^{-2} \text{d}^{-1}$ in
 396 late April (Fig. [6a5a](#)), irrespective of the total mass flux. The average 1,14-diol flux at M2 is much lower
 397 and similar for the upper and lower traps, being around $0.01\text{--}0.02 (\pm 0.01) \mu\text{g m}^{-2} \text{d}^{-1}$. At M4, the average
 398 1,14-diol fluxes are $0.3 (\pm 0.5)$ and $0.1 (\pm 0.2) \mu\text{g m}^{-2} \text{d}^{-1}$ for the upper and lower trap, respectively.
 399 There are two evident maxima in the [1,13+1,15]-diols and 1,14-diol fluxes in late April and during
 400 October/November, concomitant with maxima in the total mass flux (Fig. 3d and 3e). However, in the
 401 lower trap this flux maximum is distributed over two successive trap cups, corresponding to late
 402 April/early May (Fig. 3e and 3j).

403 The LDI ranged between 0.95 and 0.99 in all traps, corresponding to temperatures of 26.0 to 27.3 °C
404 with no particular trends (Fig. 54). For most M2 and M4 samples the C₂₈ 1,13-diol was below
405 quantification limit and, hence, LDI was always around unity, corresponding to 26.9 to 27.3 °C (Fig.
406 54), whereas in others samples the C₂₈ 1,13-diol co-eluted with cholest-5-en-7-one-3β-ol, prohibiting
407 the calculation of the LDI and Diol Index (Fig. 54 and 65). The flux-weighted annual average LDI-
408 derived SSTs are 26.6 °C for M1U, and 27.1 °C for M2U, M2L, M4U and M4L. The underlying
409 sediment is very similar, with LDI values between of 0.95 and 0.98 corresponding to 26.0 and 26.9 °C
410 (Fig. 6). The Diol Index varied from 0.03 to 0.30 in M1U, showing a pronounced maximum during
411 spring (Fig. 6a5a). The Diol Index at M2 ranges between 0.01 and 0.05 without an evident pattern, while
412 the Diol Index at M4 ranges from 0.01 to 0.10 and shows the same pattern in the lower and upper trap,
413 with highest values during spring (ca. 0.1), followed by a gradual decrease during summer (Fig. 6d5d;
414 6e5e).

415

416

3.1.2 LCAs

417 We detected C₃₇, C₃₈ and C₃₉ long-chain alkenones in the sediment trap and surface sediments. The C_{37:3}
418 alkenone was generally around the limit of quantification for the M2L and M4L traps, and below the
419 limit of quantification for 4 out of the 7 surface sediment samples, while the C_{37:2} alkenone was always
420 sufficiently abundant. The annual mean fluxes of the C₃₇ LCAs are 4.3 (± 3.5) μg m⁻² d⁻¹ for M1U, 1.2
421 (± 0.9) μg m⁻² d⁻¹ and 0.4 (± 0.2) μg m⁻² d⁻¹ for M2U and M2L, respectively, and 2.8 (± 5.0) μg m⁻² d⁻¹
422 and 1.2 (± 2.0) μg m⁻² d⁻¹ for M4U and M4L, respectively. The concentrations of the C₃₇ LCAs in the
423 underlying surface sediments range between 0.02 and 0.41 μg g⁻¹. At M4, the two total mass flux peaks
424 at the end of April and during October/November are also clearly pronounced in the C₃₇ alkenone fluxes
425 (Fig. 3d, 3e and 6g5g), as well as the increased signal in the cup reflecting the beginning of May, which
426 follows the cup which recorded the peak in total mass flux at the end of April. The U^K₃₇ varied from
427 0.87 to 0.93, corresponding to 25.1 to 27.0 °C (Fig. 7e6c) for 3 out of 7 surface sediments in which the
428 C_{37:3} was above quantification limit. The flux-weighted average SSTs are 26.1 °C for M1U, 25.7 and
429 26.4 °C for M2U and M2L, respectively, and 28.2 and 27.5 °C for M4U and M4L, respectively (Fig.

430 76). SST variations per sediment trap are generally within a 2–3 °C range (Fig. 54) with no apparent
431 trends.

432

433

3.1.3 GDGTs

434 The main GDGTs detected were the isoprenoidal GDGT-0, -1, -2, -3, crenarchaeol and the isomer of
435 crenarchaeol. Branched GDGTs were typically around or below quantification limit. ~~Additionally, we~~
436 ~~detected three hydroxyl GDGTs (OH GDGTs), i.e. OH GDGT 0, 1 and 2. These OH GDGTs~~
437 ~~contributed ca. 0.1–0.2 % to the total GDGT pool (i.e., hydroxyl and isoprenoidal) in the sediment traps,~~
438 ~~but in the surface sediments their fractional abundance was higher, around 1 %.~~ The average iGDGT
439 flux in M1U is 15.5 (\pm 4.6) $\mu\text{g m}^{-2} \text{d}^{-1}$, 2.4 (\pm 1.1) and 2.6 (\pm 0.3) $\mu\text{g m}^{-2} \text{d}^{-1}$ in M2U and M2L,
440 respectively, and 4.3 (\pm 1.5) and 2.9 (\pm 1.2) $\mu\text{g m}^{-2} \text{d}^{-1}$ in M4U and M4L, respectively (Fig. 3f). The
441 surface sediments exhibit iGDGT concentrations between 0.4 and 1.7 $\mu\text{g g}^{-1}$. Sediment $\text{TEX}_{86}^{\text{H}}$ values
442 vary between 0.62 and 0.69, corresponding to 24.3 to 27.4 °C. The $\text{TEX}_{86}^{\text{H}}$ flux-weighted average SSTs
443 are 25.2 °C for M1U, 27.3 and 26.6 °C for M2U and M2L, respectively, and 27.8 and 26.7 °C for M4U
444 and M4L, respectively. SSTs vary typically within a range of 1 and 2 °C. At M2U ~~and M4U~~, the $\text{TEX}_{86}^{\text{H}}$
445 temperatures decrease slightly (ca. 1–2 °C) ~~during-between~~ January and July (Fig. 5b ~~4~~ ~~and~~ 5d).

446

447

3.2 Mozambique Channel

448 For two time series (November 2003–September 2007 and February 2008–February 2009), we have
449 analyzed LCDs collected in the sediment trap at 2250 m water depth as well as nearby underlying surface
450 sediments (Fig. 1). The main LCDs observed in the sediment traps and surface sediments are the C_{28}
451 1,12-, 1,13- and 1,14-diols, the C_{30} 1,13-, 1,14- and 1,15-diols and the C_{32} 1,15-diol. We also observed
452 the $\text{C}_{30:1}$ 1,14 diol in some trap samples, and the C_{29} 12-OH fatty acid in all trap and sediment samples.
453 ~~The C_{30} 1,15 is generally highest in abundance, varying between 28 and 85 % of the total LCD~~
454 ~~assemblage. The C_{28} and C_{30} 1,14 diols contribute between 11 and 67 % of total LCDs.~~ In 24 samples,
455 the C_{28} 1,13-diol co-eluted with cholest-5-en-7-one-3 β -ol, and henceforth we did not calculate the LDI

456 for these samples. The C₂₈ 1,14-diol was not affected by this cholest-5-en-7-one-3 β -ol due to its much
457 higher abundance compared to the C₂₈ 1,13-diol and the Diol Index was therefore still calculated. The
458 LDI varied between 0.94 and 0.99, i.e., close to unity, corresponding to 25.5 to 27.2 °C, without an
459 evident trend (~~Fig. 8~~Fig. 7a). The Diol Index ranges between 0.11 and 0.69, showing substantial
460 variation, although not with an evident trend (~~Fig. 8~~Fig. 7b). The average LDI-derived temperature of
461 two underlying surface sediments is 26.0 °C.

462

463 3.3 Cariaco Basin

464 We analyzed LCDs for two time series (May 1999–May 2000 and July 2002–July 2003) from the upper
465 (Trap A; 275 m) and the lower trap (Trap B; 455 m) in the Cariaco Basin. The main LCDs detected for
466 both time series are the C₂₈ 1,14-, C₃₀ 1,14-, C_{30:1} 1,14-, C₂₈ 1,13-, C₃₀ 1,15- and C₃₂ 1,15-diols, as well
467 as the C₂₉ 12-OH fatty acid. ~~The C₃₀ 1,15-diol contribution varies between 3 and 92 % of all LCDs, the~~
468 ~~C₂₈ and C₃₀ 1,14-diol contribution between 3 and 96 %, and the C₂₈ and C₃₀ 1,13-diols constitute between~~
469 ~~0 and 8 %.~~ For some samples we did not compute the LDI, as the C₂₈ 1,13-diol co-eluted with cholest-
470 5-en-7-one-3 β -ol. Similarly as for the Mozambique Channel, the C₂₈ 1,14-diol was not affected by this
471 co-elution due to its much higher abundance compared to the C₂₈ 1,13-diol and the Diol Index was
472 therefore still calculated. The calculated LDI values range between 24.3 and 25.3 °C and 22.0 and 27.2
473 °C for Trap A and B of the 1999-2000 time series, respectively, with the lowest temperature during
474 winter, and the highest during summer. For the 2002-2003 time series, LDI temperatures for Trap A
475 range between 23.3 and 26.2 °C, and for Trap B between 22.5 °C and 26.5 °C.

476 For the May 1999–May 2000 time series, the Diol Index varies between 0.05 and 0.97 for Trap A, and
477 between 0.05 and 0.91 for Trap B (~~Fig. 9~~Fig. 8) with similar trends, i.e. the lowest values of around 0.1-
478 0.2 just before the upwelling period during November, rapidly increasing towards values between ca.
479 0.8 and 1 during the upwelling season (January and February). For the time series of July 2002–July
480 2003, the Diol Index shows similar trends, i.e. Diol Index values around 0.8-0.9 during July, which
481 rapidly decrease towards summer values of around 0.2-0.3. Similar to the 1999-2000 time series, the
482 lowest index values (ca. 0.2) are observed just before the upwelling period (during September), after

483 which they increase towards values of around 0.8-0.9 between December and March at the start of the
484 upwelling season. At the end of the upwelling season the Diol Index increases, followed by another
485 maximum of around 0.6 during May.

486 **4. Discussion**

487 **4.1 LCD sources and seasonality**

488 The 1,14 diols can potentially be derived from two sources, i.e. *Proboscia* diatoms (Sinninghe Damsté
489 et al., 2003; Rampen et al., 2007) or the dictyochophyte *Apedinella radians* (Rampen et al., 2011). The
490 non-detection of the C₃₂ 1,14-diol, which is a biomarker for *Apedinella radians* (Rampen et al., 2011),
491 and the detection of the C_{30:1} 1,14 diol and C₂₉ 12-OH fatty acid, which are characteristic of *Proboscia*
492 diatoms (Sinninghe Damsté et al., 2003), suggests that *Proboscia* diatoms are most likely the source of
493 1,14-diols in the tropical North Atlantic, the Mozambique Channel and the Cariaco Basin.

494 In the Cariaco Basin, the Diol Index shows a strong correlation (visually as correlation analysis was not
495 possible due to differently spaced data in time)-with primary production rates, suggesting that *Proboscia*
496 productivity was synchronous with total productivity (Fig. 9Fig. 8), although for the 1999-2000 time
497 series there is a disagreement during January/February. Primary productivity in the Cariaco Basin is
498 largely related to seasonal upwelling which occurs between November and May when the ITCZ is at its
499 southern position. Hence, the Diol Index seems to be an excellent indicator of upwelling intensity in the
500 Cariaco Basin.

501 The index also shows considerable variation over time in the Mozambique Channel (Fig. 8Fig. 7b).
502 Previous studies have shown that upwelling occurs in the Mozambique Channel between ca. 15 and
503 18°S (Nehring et al., 1987; Malauene et al., 2014), i.e. at the location of our sediment trap. Upwelling
504 is reflected by cool water events and slightly enhanced Chlorophyll *a* levels, and Malauene et al. (2014)
505 observed cool water events at ca. two month intervals although periods of 8 to 30 days were also
506 observed. The two main potential forcing mechanisms for upwelling in the Mozambique Channel are
507 the East African monsoon winds and the meso-scale eddies migrating through the channel. Fallet et al.
508 (2011) showed that subsurface temperature, current velocity and the depth of surface-mixed layer all

509 revealed a dominant periodicity of four to six cycles per year, which is the same frequency as that of the
510 southward migration of meso-scale eddies in the channel (Harlander et al., 2009; Ridderinkhof et al.,
511 2010), implying that eddy passage strongly influences the water mass properties. Wavelet analysis of
512 the Diol Index for the period 2003–2007 (~~not shown~~ [supplemental Fig. S1](#)) revealed short periods,
513 occurring around January of 2004, 2005, and 2006, of significant (above the 95 % confidence level)
514 variability at about bimonthly frequencies (60-day period). Both the frequency ([bimonthly](#)) and the
515 timing ([boreal winter](#)) of the observed time periods of enhanced Diol Index variability are similar to
516 those of the cool water events as observed by Malauene et al. (2014), associated with upwelling ([Fig.](#)
517 [8Fig. 7b](#)). The strongest variability of the Diol Index at ~~frequencies of four cycles~~ [about bimonthly](#)
518 ~~frequencies per year and higher~~ occurred in the first half of 2006. During the same period, salinity time
519 series showed the passage of several eddies that had a particularly strong effect on the upper layer
520 hydrography (Ullgren et al., 2012). Malauene et al. (2014) showed that neither upwelling-favorable
521 winds, nor passing eddies, can by themselves explain the observed upwelling along the northern
522 Mozambique coast. The two processes may act together, and both strongly influence the upper water
523 layer and the organisms living there, potentially including the LCD producers.

524 The least (seasonal) variation in the Diol Index is observed at M2 in the tropical North Atlantic ([Fig. 6b](#)
525 [5b](#) and [5c](#)), which is likely due to its central open ocean position, associated with relatively stable,
526 oligotrophic conditions (Guerreiro et al., 2017). In contrast, M4 and M1 are closer to the south American
527 and west African coast, respectively, and thus are potentially under the influence of Amazon river runoff
528 and upwelling, respectively, and specific wind and ocean circulation regimes (see Sect. 2.1.1). However,
529 at M4, the Diol Index is also low (max. 0.1), suggesting low *Proboscia* productivity ([Fig. 6d](#) [5d](#) and [5e](#)).
530 At M1, by contrast, we observe enhanced values for the Diol Index of up to ~0.3 during spring ([Fig.](#)
531 [6a](#) [5a](#)). Most likely, an upwelling signal at this location is associated with the seasonal upwelling of the
532 Guinea Dome. This upwelling is generally most intense between July and October (Siedler et al., 1992),
533 due to the northward movement of the ITCZ and the resulting intensified Ekman upwelling. Specifically,
534 during this period, the trade winds are weaker, atmospheric pressure is lower, and the regional wind
535 stress is favorable to upwelling of the North Equatorial Undercurrent (Voituriez, 1981). Indeed, a

536 decrease in wind speed and increased precipitation during summer to autumn was observed (Fig. 6a5a)
537 which confirms that during these seasons the ITCZ was indeed at a northern position, and that during
538 2013 the upwelling associated with the Guinea Dome was most favored between July and October. The
539 timing of the Diol Index peak, i.e., between March and June is consistent with previous sediment trap
540 studies elsewhere which have shown that *Proboscia* diatoms and 1,14-diols are typically found during
541 pre-upwelling or early upwelling periods (Koning et al., 2001; Smith, 2001; Sinninghe Damsté et al.,
542 2003; Rampen et al., 2007). The surface sediment at 22° W just east of M1 also reveals the highest Diol
543 Index (0.53), likely due to its closer vicinity to the Guinea Dome center. Several studies have reported
544 *P. alata* diatoms offshore North West Africa (Lange et al., 1998; Treppke et al., 1995; Crosta et al.,
545 2012; Romero et al., 1999), pointing to *P. alata* as a plausible source organism. The sedimentary annual
546 diol indices compare well with the sediment trap indices (Fig. 7e6e), which is consistent with the results
547 of Rampen et al. (2008). Our results clearly show that the Diol Index reflects different things in different
548 regions. This is due to the ecology of *Proboscia* spp. where blooms occur during stratification to early
549 upwelling to postbloom, and from high nutrients to low nutrients (see Rampen et al., 2014; references
550 in Table 1). Therefore, the type of conditions reflected by the Diol Index is specific for every region.
551 To assess variations in seasonal production of 1,13- and 1,15-diols in the tropical Atlantic, for which we
552 have the most complete dataset, we calculated the flux-weighted 1,13- and 1,15-diol concentrations for
553 the different traps, and summed these per season (Fig. 49). Highest production is observed in autumn,
554 followed by summer and spring, with the lowest production during winter (~60 % compared to autumn).
555 This is in agreement with Rampen et al. (2012) who observed, for an extensive set of surface sediments,
556 the strongest correlation between LDI and SST for autumn, suggesting that production of the source
557 organisms of the LDI mainly occurs during autumn. At M4, there are two evident peaks in the 1,13- and
558 1,15-diol fluxes at the end of April and October 2013. These maxima correlate with peaks in other lipid
559 biomarker fluxes (i.e., 1,14-diols, C₃₇ alkenones and iGDGTs), total mass flux, calcium carbonate
560 (CaCO₃), OM and the residual mass flux which includes the deposition flux of Saharan dust (Korte et
561 al., 2017). According to Guerreiro et al. (2017), the maximum in total mass flux at the end of April 2013
562 is likely caused by enhanced export production due to nutrient enrichment as a result of wind-forced

563 vertical mixing. The peak at the end of October 2013, is likely associated with discharge from the
564 Amazon River. Moreover, both peaks are concomitant with prominent dust flux maxima, suggesting
565 that Saharan dust also acted as nutrient fertilizer (Korte et al., 2017; Guerreiro et al., 2017). Guerreiro
566 et al. (2017) suggested that during the October-November event the Amazon River may not only have
567 acted as nutrient supplier, but also as buoyant surface density retainer of dust-derived nutrients in the
568 surface waters, resulting in the development of algal blooms within just a few days, potentially
569 explaining the peak 1,13- and 1,15-diol fluxes, as well as the peak fluxes of the other lipid biomarkers.
570 However, they might also partially result from enhanced particle settling, caused by e.g. dust ballasting
571 or faecal pellets of zooplankton (see Guerreiro et al. 2017 and references therein). This agrees with the
572 results of Schreuder et al. (2018a) who show that the *n*-alkane flux also peaks concomitant with the
573 peaks in total mass flux and biomarkers, whereas *n*-alkanes are terrestrial derived (predominantly
574 transported by dust) and increased deposition can therefore not result from increased primary
575 productivity in the surface waters.

576 The C₃₇ alkenone flux at M4U also reveals these two distinct maxima at the end of April and October
577 during 2013 (Fig. 6g5g). Interestingly, this flux, as well as the alkenone flux at M2U, is consistent with
578 coccolith export fluxes of the species *Emiliania huxleyi* and *Gephyrocapsa oceanica* (Guerreiro et al.,
579 2017). In fact, when we combine the coccolith fluxes of both species, we observe strong correlations
580 with the C₃₇ alkenone fluxes for both M2U and M4U (Fig. 6f5f and 6g5g, respectively; $R^2 = 0.60-77$
581 and $0.84-92$ for M2U and M4U, respectively; p -values < 0.001). This implies that these two species are
582 the main LCA producers in the tropical North Atlantic, which agrees with previous findings (e.g.,
583 Marlowe et al., 1984; Brassell, 2014; Conte et al., 1994; Volkman et al., 1995).

584

585 4.2 Preservation of LCDs

586 The sediment trap data from the North Atlantic can be used to assess the relative preservation of LCDs,
587 as well as other proxy lipid biomarkers, by comparing the flux-weighted concentration in the traps with
588 the concentrations in the surface sediments. For all four biomarker groups, i.e., C₃₇ alkenones, iGDGTs,
589 1,14-diols and 1,13- and 1,15-diols, we observe that in general the flux-weighted concentrations are

590 higher in the upper traps (ca. 1200 m) as compared to the lower traps (ca. 3500 m; Fig. 2) by a factor of
591 between 1.2 and 4.4, implying degradation during settling down the water column. The concentrations
592 in the surface sediments are 2 to 3 orders of magnitude lower in concentration (i.e., between 0.1–1.5 %
593 of upper trap signal), implying that degradation of lipids is mainly taking place at the water-sediment
594 surface rather than the water column. A similar observation was made for levoglucosan in these sediment
595 traps (Schreuder et al., 2018b). Both are functionalized polar lipids with alcohol groups and thus are
596 chemically relatively similar when compared to e.g. fatty acids (carboxyl group) or *n*-alkanes (no
597 functional groups). ~~This~~ These is degradation rates are likely linked to the extent of the oxygen exposure
598 time (Hartnett et al., 1998; Hedges et al., 1999) at the seafloor (Hartnett et al., 1998; Sinninghe Damsté
599 et al., 2002), since during settling the lipids are exposed to oxygen for weeks, whereas for surface
600 sediments this is typically decades to centuries. Our results compare well with several other sediment
601 trap studies which showed that LCDs, LCAs and iGDGTs generally have a preservation factor of around
602 1 % (surface sediment vs. trap) (e.g., Prahl et al., 2000; Wakeham et al., 2002; Rampen et al., 2007;
603 Yamamoto et al., 2012).

604 We have also identified the C₃₀ and C₃₂ 1,15-keto-ol ~~for~~ in the Atlantic as well as the Mozambique and
605 Cariaco sediment traps and surface sediments. These lipids are structurally related to LCDs and occur
606 ubiquitously in marine sediments (e.g., Versteegh et al., 1997; 2000; Bogus et al., 2012; Rampen et al.,
607 2007; Sinninghe Damsté et al., 2003; Wakeham et al., 2002; Jiang et al., 1994), and were inferred to be
608 oxidation products of LCDs (Ferreira et al., 2001; Bogus et al., 2012; Sinninghe Damsté et al., 2003).
609 We have not detected 1,14-keto-ols, which supports the hypothesis of Ferreira et al. (2001) and
610 Sinninghe Damsté et al. (2003) that the silica frustules of *Proboscia* diatoms sink relatively fast and thus
611 are exposed to oxygen for a shorter period than the producers of 1,13- and 1,15-diols, and thus less
612 affected by oxidation. Alternatively, the keto-ols are not oxidation products but are produced by
613 unknown organisms in the water column. In fact, Méjanelle et al. (2003) observed trace amounts of C₃₀
614 1,13- and C₃₂ 1,15-keto-ols in cultures of the marine eustigmatophyte *Nannochloropsis gaditana*. Thus,
615 an alternative explanation for the non-detection of 1,14-keto-ols is that, in contrast to the 1,15-keto-ols,
616 they were not produced in the water column.

617 For both the tropical Atlantic and the Cariaco Basin, we observe highly similar LDI values for the upper
618 and the lower traps. In the Atlantic there is no statistical difference between upper and lower trap that
619 are 2200 m apart (two-tailed $p > 0.8$), but we have too little data for the Cariaco Basin for statistical
620 comparison (Fig. [7b6b](#), [9e-8c](#) and [9f8f](#)). This suggests that degradation in the water column does not
621 affect the LDI proxy. This is in agreement with the study of Reiche et al. (2018) who performed a short-
622 term degradation experiment (< 1 year) and found that the LDI index was not affected by oxic exposure
623 on short time scales. However, the oxygen exposure time on the seafloor is much longer, and Rodrigo-
624 Gámiz et al. (2016) showed for sediments in the Arabian Sea, deposited under a range of bottom water
625 oxygen conditions, that different LCDs had different degradation rates, which compromised the LDI
626 ratio. For the three sites in the tropical North Atlantic, we have calculated the flux-weighted average
627 proxy values for every sediment trap and compare these with the underlying surface sediments (Fig.
628 [7b6b-7e6e](#)). For all indices, i.e., Diol Index, LDI, U^{K}_{37} and TEX_{86} , we observe very good
629 correspondence between the sediment trap and surface sediment values, implying minimal alteration of
630 the proxies after settling and during burial. Similarly, for the Mozambique Channel, the mean Diol Index
631 and LDI from the sediment trap (i.e., 0.41 and 0.97, respectively) are very similar to the surface sediment
632 values (i.e., 0.42 and 0.95, respectively). In agreement with the consistent diol indices, we observe that
633 all individual LCDs are also preserved relatively equally in the tropical Atlantic (1.2-4.3 % at station
634 M1, 0.1-2.9 % at station M2 and 0.03-0.16 % at station M4). This contrasts with the findings of Rodrigo-
635 Gámiz et al. (2016) who found that the 1,15-diols have the highest degradation rate, followed by the
636 1,14- and 1,13-diols. Only the C_{32} 1,15-diol seems relatively better preserved than the other LCDs at all
637 three North Atlantic mooring sites (Fig. 2), suggesting that the C_{32} 1,15-diol is less impacted by
638 degradation. The C_{32} 1,15-diol likely partially derives from the same source as the other 1,13- and 1,15-
639 diols, but is also produced in fresh water systems (e.g., Versteegh et al., 1997; 2000; Rampen et al.,
640 2014b; de Bar et al., 2016; Lattaud et al., 2017a; 2017b). Hence, the different preservation characteristics
641 might be the result of a different source for this LCD.

642

643

4.3 Relationship between LDI and SST

644 In the tropical Atlantic and Mozambique Channel, the LDI-derived SSTs show minimal **differences**
645 **variability** (<2 °C), while in the Cariaco Basin we observe much larger changes that range from 22.0 °C
646 to 27.2 °C (~~Fig. 9~~**Fig. 8**). Both time series in the Cariaco Basin show low temperatures between
647 November and May associated with the seasonal upwelling and surface water cooling, and significantly
648 higher temperatures during the rainy summer. However, during the warmest periods, the LDI
649 temperatures are generally lower than measured at the surface by CTD, whereas during the colder
650 phases, the LDI agrees well with the measurements. The LDI calibration reaches unity at 27.4 °C, and
651 therefore it is not possible to resolve the highest temperatures which are between ca. 28 and 30 °C.
652 However, the LDI-derived temperatures are sometimes well below 27.4 °C where the CTD data suggest
653 SSTs > 28 °C. Consequently, the LDI-based temperatures agree with CTD-based SSTs within
654 calibration error for most of the record, but during summer when SST is highest, are offset outside the
655 calibration error ($\Delta T \sim 2.5$ ~~4.5~~ °C). Interestingly, the $U^{K'_{37}}$ - and $TEX^{H_{86}}$ -derived temperature trends show
656 the same phenomenon (Turich et al., 2013; ~~Fig. 9~~**Fig. 8**), where the proxy temperatures are cooler than
657 the measured temperatures during the warmer months. However, in contrast to the $U^{K'_{37}}$ and LDI, the
658 $TEX^{H_{86}}$ also overestimates SST- during the cold months. For $U^{K'_{37}}$, Turich et al. (2013) pointed out that
659 a time lag between synthesis, export and deposition could potentially explain the difference between the
660 proxy and CTD temperatures. However, previous analysis of plankton biomass, primary productivity,
661 bio-optical properties and particulate organic carbon fluxes for the same time period (Müller-Karger et
662 al., 2004), as well as the total mass and terrigenous fluxes assessed by Turich et al. (2013) showed best
663 correlation at zero-time lag on the basis of their 14-day sample interval. We compared our LDI
664 temperature estimates with monthly CTD measurements between 0 and 50 m depth, the temperature at
665 depth of maximum primary productivity and the temperature at the chlorophyll maximum (Turich et al.,
666 2013; <http://www.imars.usf.edu/cariaco>) (Fig. 10). During the upwelling season, temperatures are
667 significantly lower due to the upward migration of isotherms, whereas during the non-upwelling period,
668 temperatures are higher, particularly in the upper 20 m, and the water column is more stratified (Fig.
669 10). LDI underestimates SST during stratification, which suggests that the LCD producers may thrive
670 at depths of ca. 20–30 m. During upwelling, LDI-temperatures agree better with SST, implying that the

671 habitat of the LCD producers potentially was closer to the surface, coincident with the shoaling of the
672 nutricline and thermocline (Fig. 10). However, these absolute differences in LDI-temperatures are
673 generally within the calibration error (2 °C), and these seasonal variations in LDI-temperatures should
674 thus be interpreted with caution. Turich et al. (2003) found that the $U^{K'}_{37}$ -derived temperatures agreed
675 reasonably well with the measured temperatures at the chlorophyll maximum, which is generally found
676 below 20 m depth (average 30–34 m depth; ranging between 1 and 55 m) in the Cariaco Basin. The LDI
677 temperatures are almost always higher than the temperatures at the chlorophyll maximum (Fig. 10), and
678 higher than the temperatures at 30 m depth, implying that the LDI producers may reside in the upper 30
679 m of the water column, which is consistent with the results of Rampen et al. (2012), who showed that
680 LDI-derived temperatures have the strongest correlation with temperatures of the upper 20 m of the
681 water column. This also agrees with Balzano et al. (2018) who observed highest LCD abundances within
682 the upper 20 m of the water column in the Tropical Atlantic.

683 In the Mozambique Channel, the LDI temperature variations are much smaller (< 2 °C; ~~Fig. 8~~Fig. 7a)
684 than the seasonal SST variation ranging between ca. 24.5 and 30.5 °C. Accordingly, during the warmest
685 months of the year, the difference between LDI-derived and satellite-derived SST is outside of the
686 calibration error (i.e., > 2 °C). However, this is similar to the $U^{K'}_{37}$ and TEX^{H}_{86} which also did not reveal
687 seasonal variations. This lack of seasonality was explained by lateral advection and re-suspension of
688 fine sediment material by migrating meso-scale eddies and thus ending up in the deeply moored
689 sediment trap (Fallet et al., 2011; 2012). Most likely, this also explains the lack of seasonal variation in
690 our LDI record (~~Fig. 8~~Fig. 7a). Nevertheless, the average LDI temperature for the sediment trap of 26.4
691 °C agrees reasonably well with the annual mean satellite-derived SST of 27.6 °C for the sampled years.
692 Additionally, there is a good agreement with the average LDI temperature of 26.0 °C for two underlying
693 surface sediments, as well as with the decadal average SST of 26.7 °C for 1955-2012 (Locarnini et al.,
694 2013) given by the World Ocean Atlas (2013). For the North Atlantic, we also observe rather constant
695 LDI temperatures during the year (Fig. 54) which contrasts with seasonal variations in satellite SSTs of
696 ca. 3 to 5 °C. Nevertheless, differences are mostly within the calibration error, except at M1 and M2
697 where during winter and spring LDI-derived temperatures are between 0.5 and 2.8 °C higher than

698 satellite SSTs. Similar to the LDI, also the $\text{TEX}^{\text{H}}_{86}$ and U^{K}_{37} -derived SSTs for the tropical Atlantic
699 sediment traps do not reveal clear seasonal variation. As all three proxies show minimal seasonal
700 variability, this might indicate that the lipids are potentially allochthonous and partially derive from
701 distant regions, resulting in an integrated average temperature signal, similar to the Mozambique
702 Channel. Nevertheless, the flux-weighted annual LDI temperatures of the tropical Atlantic sediment
703 traps (26.6 for M1 and 27.1 °C for M2 and M4) agree well with the annual mean satellite-derived SSTs
704 of 26.1, 26.0 and 27.5 °C for M1, M2 and M4, respectively. Moreover, the LDI-derived temperatures in
705 the underlying sediments (26.5, 26.6 and 26.7 °C, respectively) do not only agree well with those found
706 in a single year in the sediment traps but also with the decadal average SSTs for 1955 to 2012 (26.2,
707 27.1 and 26.3 °C, respectively; Locarnini et al., 2013; Fig. 7b6b).

708

709 ~~Interestingly, $\text{TEX}^{\text{H}}_{86}$ temperature estimates are relatively similar for traps M2 and M4 but at M1 they~~
710 ~~are lower than satellite SST in both the sediment trap and surface sediments (Fig. 7d). This~~
711 ~~underestimation of SST at M1 might suggest GDGT addition from colder subsurface waters. Indeed~~
712 ~~Balzano et al. (unpublished results) show that crenarchaeol is typically abundant between ca. 40 and~~
713 ~~100 m water depth, agreeing with previous findings which have shown that the TEX_{86} can reflect~~
714 ~~subsurface temperatures rather than surface temperature in some regions (e.g., Huguet et al., 2007; Kim~~
715 ~~et al., 2012; 2015; Schouten et al., 2013; Chen et al., 2014; Wuchter et al., 2006). Consequently, for the~~
716 ~~surface sediments, we also calculated subsurface temperatures, using the calibration of Kim et al. (2012)~~
717 ~~(Fig. 7d), and compared these with the depth integrated annual mean temperatures of the upper 150 m~~
718 ~~(Locarnini et al., 2013), calculated following Kim et al. (2008), which indeed shows a better~~
719 ~~correspondence for the eastern Atlantic surface sediment, i.e., the sediments close to M1. This is likely~~
720 ~~caused by the steepening of the thermocline towards the east, as shown in Fig. 7a,d, in which we have~~
721 ~~indicated the approximate production depths of the temperature proxies. The thermocline at M1 is much~~
722 ~~steeper and shallower, which implies that GDGTs produced at ~100 m depth will record a lower~~
723 ~~temperature than at M2 and M4.~~

724

725 5. Conclusions

726 In this study we have evaluated LCD-based proxies, particularly the LDI, in sediment trap time series
727 from five sites in the tropical North Atlantic, the Cariaco Basin and the Mozambique Channel. For the
728 North Atlantic we found that in the water column ca. 25–85 % of the export of these lipid biomarkers is
729 preserved during settling from 1200m to 3500m, and that generally less than 2 % was preserved in the
730 surface sediments. Despite substantial degradation at the seafloor, likely linked to the prolonged oxygen
731 exposure time, LCD-derived temperatures from the sediments are generally very similar to the annual
732 mean LCD-derived temperatures in both the deep and shallow traps as well as to annual mean SST for
733 the specific sampling year and on decadal time scales for the specific sites. In the Cariaco Basin we
734 observe a ~~strong seasonality~~seasonal signal in the LDI ~~which is~~ linked to the upwelling season ~~at~~
735 reflecting temperatures ~~associated with a water depth of up to ca. 30 m during summer~~
736 ~~stratification, and at SST during winter upwelling accompanied by shoaling of both the nutricline and~~
737 isotherms of the water column. The LDI temperatures in the Mozambique Channel and the tropical
738 Atlantic reveal minimal seasonal change although seasonal SST contrasts amount to 3-5°C. For the
739 Mozambique Channel this is likely caused by lateral advection of re-suspended sediment by meso-scale
740 eddy migration, a signal not substantially altered by diagenesis. Seasonal variations in the Diol Index
741 are minimal in the central and western North Atlantic and 1,14-diol concentrations are rather low,
742 implying little *Proboscia* diatom productivity. However, in the eastern Atlantic closest to the African
743 continent, the Diol Index attains a clear spring maximum that is likely associated with upwelling in the
744 Guinea Dome during summer to autumn, suggesting the Diol Index reflects a pre-upwelling signal,
745 consistent with the current knowledge on *Proboscia* ecology. In the Cariaco Basin, controlled by
746 seasonal upwelling, the Diol Index reveals the same clear seasonal trend observed in primary
747 productivity, arguing that for this location the Diol Index is an excellent indicator of upwelling intensity.

748

749 **Data availability.** The data reported in this paper is archived in PANGAEA (www.pangaea.de.)

750

751 **Author contributions.** MWdB, JSSD, and SS designed the experiments and MWdB carried them out.
752 JU carried out the time-series analysis. JBWS, GJAB, and RCT deployed sediment traps and collected
753 sediment trap materials. MWdB prepared the paper with contributions from all coauthors.

754

755 **Competing interests.** The authors declare that they have no conflict of interest.

756

757 **Acknowledgements.** We are grateful to Laura Schreuder and Denise Dorhout for analytical support,
758 Wim Boer for help with MatLab calculations (BAYSPLINE), Laura Korte and Catarina Guerreiro for
759 constructive discussions, and Isla Castañeda, Ulrike Fallet and Courtney Turich for providing and
760 working up samples. This research has been funded by the European Research Council (ERC) under the
761 European Union's Seventh Framework Program (FP7/2007-2013) ERC grant agreement [339206] to
762 S.S. and ERC grant agreement [311152] as well as NWO project [822.01.008] to J-B.S.. S.S. and
763 J.S.S.D. receive financial support from the Netherlands Earth System Science Centre (NESSC) through
764 a gravitation grant from the Dutch ministry for Education, Culture and Science (grant number
765 024.002.001).

766

767 **References**

768 Araujo, M., Noriega, C., Hounsou-gbo, G. A., Veleda, D., Araujo, J., Bruto, L., Feitosa, F.,
769 Flores-Montes, M., Lefevre, N., Melo, P., Otsuka, A., Travassos, K., Schwamborn, R., and Neumann-
770 Leitao, S.: A Synoptic Assessment of the Amazon River-Ocean Continuum during Boreal Autumn:
771 From Physics to Plankton Communities and Carbon Flux, *Front. Microbiol.*, 8,
772 <https://doi.org/10.3389/fmicb.2017.01358>, 2017.

773 Balzano, S., Lattaud, J., Villanueva, L., Rampen, S. W., Brussaard, C. P. D., van Bleijswijk, J.,
774 Bale, N., Sinninghe Damsté, J. S., and Schouten, S.: A quest for the biological sources of long chain
775 alkyl diols in the western tropical North Atlantic Ocean, *Biogeosciences*, 15, 5951-5968,
776 <https://doi.org/10.5194/bg-15-5951-2018>, 2018.

777 Biastoch, A., and Krauss, W.: The Role of Mesoscale Eddies in the Source Regions of the
778 Agulhas Current, *J. Phys. Oceanogr.*, 29, 2303-2317, [https://doi.org/10.1175/1520-0485\(1999\)029<2303:Tromei>2.0.Co;2](https://doi.org/10.1175/1520-0485(1999)029<2303:Tromei>2.0.Co;2), 1999.

780 Bogus, K. A., Zonneveld, K. A. F., Fischer, D., Kasten, S., Bohrmann, G., and Versteegh, G. J.
781 M.: The effect of meter-scale lateral oxygen gradients at the sediment-water interface on selected
782 organic matter based alteration, productivity and temperature proxies, *Biogeosciences*, 9, 1553-1570,
783 <https://doi.org/10.5194/bg-9-1553-2012>, 2012.

784 Brassell, S. C., Eglinton, G., Marlowe, I. T., Pflaumann, U., and Sarnthein, M.: Molecular
785 stratigraphy – A new tool for climatic assessment, *Nature*, 320, 129-133,
786 <https://doi.org/10.1038/320129a0>, 1986.

787 Brassell, S. C.: Climatic influences on the Paleogene evolution of alkenones, *Paleoceanography*,
788 29, 255-272, <https://doi.org/10.1002/2013pa002576>, 2014.

789 Chen, W. W., Mohtadi, M., Schefuss, E., and Mollenhauer, G.: Organic-geochemical proxies
790 of sea surface temperature in surface sediments of the tropical eastern Indian Ocean, *Deep-Sea Res. Pt.*
791 *I*, 88, 17-29, <https://doi.org/10.1016/j.dsr.2014.03.005>, 2014.

792 Coles, V. J., Brooks, M. T., Hopkins, J., Stukel, M. R., Yager, P. L., and Hood, R. R.: The
793 pathways and properties of the Amazon River Plume in the tropical North Atlantic Ocean, *J. Geophys.*
794 *Res-Oceans*, 118, 6894-6913, <https://doi.org/10.1002/2013jc008981>, 2013.

795 Conte, M. H., Thompson, A., and Eglinton, G.: Primary production of lipid biomarker
796 compounds by *Emiliana Huxleyi* – Results from an experimental mesocosm study in fjords of
797 southwestern Norway, *Sarsia*, 79, 319-331, <https://doi.org/10.1080/00364827.1994.10413564>, 1994.

798 Conte, M. H., Sicre, M. A., Ruhlemann, C., Weber, J. C., Schulte, S., Schulz-Bull, D., and
799 Blanz, T.: Global temperature calibration of the alkenone unsaturation index $U^{K'}_{37}$ in surface waters and
800 comparison with surface sediments, *Geochem. Geophys. Geosy.*, 7,
801 <https://doi.org/10.1029/2005GC001054>, 2006.

802 Cropper, T. E., Hanna, E., and Bigg, G. R.: Spatial and temporal seasonal trends in coastal
803 upwelling off Northwest Africa, 1981-2012, *Deep-Sea Res. Pt. I*, 86, 94-111,
804 <https://doi.org/10.1016/j.dsr.2014.01.007>, 2014.

805 Crosta, X., Romero, O. E., Ther, O., and Schneider, R. R.: Climatically-controlled siliceous
806 productivity in the eastern Gulf of Guinea during the last 40 000 yr, *Clim. Past*, 8, 415-431,
807 <https://doi.org/10.5194/cp-8-415-2012>, 2012.

808 de Bar, M. W., Dorhout, D. J. C., Hopmans, E. C., Rampen, S. W., Sinninghe Damsté, J. S., and
809 Schouten, S.: Constraints on the application of long chain diol proxies in the Iberian Atlantic margin,
810 *Org. Geochem.*, 101, 184-195, <https://doi.org/10.1016/j.orggeochem.2016.09.005>, 2016.

811 de Jonge, C., Hopmans, E. C., Zell, C. I., Kim, J. H., Schouten, S., and Sinninghe Damsté, J. S.:
812 Occurrence and abundance of 6-methyl branched glycerol dialkyl glycerol tetraethers in soils:
813 Implications for palaeoclimate reconstruction, *Geochim. Cosmochim. Ac.*, 141, 97-112,
814 <https://doi.org/10.1016/j.gca.2014.06.013>, 2014.

815 de Jonge, C., Stadnitskaia, A., Hopmans, E. C., Cherkashov, G., Fedotov, A., Streletskaia, I.
816 D., Vasiliev, A. A., and Sinninghe Damsté, J. S.: Drastic changes in the distribution of branched
817 tetraether lipids in suspended matter and sediments from the Yenisei River and Kara Sea (Siberia):
818 Implications for the use of brGDGT-based proxies in coastal marine sediments, *Geochim. Cosmochim.*
819 *Ac.*, 165, 200-225, <https://doi.org/10.1016/j.gca.2015.05.044>, 2015.

820 Doi, T., Tozuka, T., and Yamagata, T.: Interannual variability of the Guinea Dome and its
821 possible link with the Atlantic Meridional Mode, *Clim. Dynam.*, 33, 985-998,
822 <https://doi.org/10.1007/s00382-009-0574-z>, 2009.

823 Duce, R. A., Liss, P. S., Merrill, J. T., Atlas, E. L., Buat-Menard, P., Hicks, B. B., Miller, J. M.,
824 Prospero, J. M., Arimoto, R., Church, T. M., Ellis, W., Galloway, J. N., Hansen, L., Jickells, T. D.,
825 Knap, A. H., Reinhardt, K. H., Schneider, B., Soudine, A., Tokos, J. J., Tsunogai, S., Wollast, R., and
826 Zhou, M.: The Atmospheric Input of Trace Species to the World Ocean, *Global Biogeochem. Cy.*, 5,
827 193-259, <https://doi.org/10.1029/91gb01778>, 1991.

828 Fallet, U., Brummer, G. J., Zinke, J., Vogels, S., and Ridderinkhof, H.: Contrasting seasonal
829 fluxes of planktonic foraminifera and impacts on paleothermometry in the Mozambique Channel
830 upstream of the Agulhas Current, *Paleoceanography*, 25, 12, <https://doi.org/10.1029/2010pa001942>,
831 2010.

832 Fallet, U., Ullgren, J. E., Castaneda, I. S., van Aken, H. M., Schouten, S., Ridderinkhof, H., and
833 Brummer, G. J. A.: Contrasting variability in foraminiferal and organic paleotemperature proxies in
834 sedimenting particles of the Mozambique Channel (SW Indian Ocean), *Geochim. Cosmochim. Ac.*, 75,
835 5834-5848, <https://doi.org/10.1016/j.gca.2011.08.009>, 2011.

836 Fallet, U., Castaneda, I. S., Aneurin, H. E., Richter, T. O., Boer, W., Schouten, S., and Brummer,
837 G. J.: Sedimentation and burial of organic and inorganic temperature proxies in the Mozambique
838 Channel, SW Indian Ocean, *Deep-Sea Res. Pt. I*, 59, 37-53, <https://doi.org/10.1016/j.dsr.2011.10.002>,
839 2012.

840 Ferreira, A. M., Miranda, A., Caetano, M., Baas, M., Vale, C., and Sinninghe Damsté, J. S.:
841 Formation of mid-chain alkane keto-ols by post-depositional oxidation of mid-chain diols in
842 Mediterranean sapropels, *Org. Geochem.*, 32, 271-276, [https://doi.org/10.1016/S0146-6380\(00\)00181-](https://doi.org/10.1016/S0146-6380(00)00181-9)
843 9, 2001.

844 Frouin, R., Franz, B. A., Werdell, P. J.: The SeaWiFS PAR product., In: S.B. Hooker and E.R.
845 Firestone, Algorithm Updates for the Fourth SeaWiFS Data Reprocessing, NASA Tech. Memo. 2003–
846 206892, Volume 22, NASA Goddard Space Flight Center, Greenbelt, Maryland, 46-50. The SeaWiFS
847 PAR product, 2003.

848 Gibbons, J. D. & Chakraborty, S.: Nonparametric Statistical Inference. Fourth Edition. Marcel
849 Dekker Inc., New York, 645 pp. ISBN: 0-8247-4052-1, 2003.

850 Goddard Earth Sciences Data and Information Services Center, TRMM (TMPA-RT) Near Real-
851 Time Precipitation L3 1 day 0.25 degree x 0.25 degree V7, Greenbelt, MD, Goddard Earth Sciences
852 Data and Information Services Center (GES DISC),
853 http://disc.gsfc.nasa.gov/datacollection/TRMM_3B42RT_Daily_7.html, 2016.

854 Goñi, M. A., Woodworth, M. P., Aceves, H. L., Thunell, R. C., Tappa, E., Black, D., Müller-
855 Karger, F., Astor, Y., and Varela, R.: Generation, transport, and preservation of the alkenone-based $U^{K_{37}}$
856 sea surface temperature index in the water column and sediments of the Cariaco Basin (Venezuela),
857 *Global Biogeochem. Cy.*, 18, 1-21, <https://doi.org/10.1029/2003GB002132>, 2004.

858 Gordon, A. L.: Inter-ocean exchange of thermocline water, *J. Geophys. Res-Oceans*, 91, 5037-
859 5046, <https://doi.org/10.1029/JC091iC04p05037>, 1986.

860 Goudie, A. S., and Middleton, N. J.: Saharan dust storms: nature and consequences, *Earth-Sci.*
861 *Rev.*, 56, 179-204, [https://doi.org/10.1016/S0012-8252\(01\)00067-8](https://doi.org/10.1016/S0012-8252(01)00067-8), 2001.

862 Guerreiro, C. V., Baumann, K. H., Brummer, G. J. A., Fischer, G., Korte, L. F., Merkel, U., Sa,
863 C., de Stigter, H., and Stuut, J. B. W.: Coccolithophore fluxes in the open tropical North Atlantic:
864 influence of thermocline depth, Amazon water, and Saharan dust, *Biogeosciences*, 14, 4577-4599,
865 <https://doi.org/10.5194/bg-14-4577-2017>, 2017.

866 Guerreiro, C. V., Baumann, K.-H., Brummer, G.-J. A., Fischer, G., Korte, L. F., Sá, C. and
867 Stuut, J.-B. W.: Wind-forced transatlantic gradients in coccolithophore species fluxes, Submitted to
868 *Prog. Oceanogr.* (in revision), 2018.

869 Harlander, U., Ridderinkhof, H., Schouten, M. W., and de Ruijter, W. P. M.: Long-term
870 observations of transport, eddies, and Rossby waves in the Mozambique Channel, *J. Geophys. Res-*
871 *Oceans*, 114, <https://doi.org/10.1029/2008jc004846>, 2009.

872 Hartnett, H. E., Keil, R. G., Hedges, J. I., and Devol, A. H.: Influence of oxygen exposure time
873 on organic carbon preservation in continental margin sediments, *Nature*, 391,
874 <https://doi.org/10.1038/35351> 572-574, 1998.

875 Hedges, J. I., Sheng Hu, F., Devol, A. H., Hartnett, H. E., Tsamakis, E., and Keil, R. G.:
876 Sedimentary organic matter preservation: a test for selective degradation under oxic conditions, *Am. J.*
877 *Sci.*, 299, 529-555, <https://doi.org/10.2475/ajs.299.7-9.529> 1999.

878 Herndl, G. J., Reinthaler, T., Teira, E., van Aken, H., Veth, C., Pernthaler, A., and Pernthaler,
879 J.: Contribution of *Archaea* to total prokaryotic production in the deep Atlantic Ocean, *Appl. Environ.*
880 *Microb.*, 71, 2303-2309, <https://doi.org/10.1128/aem.71.5.2303-2309.2005>, 2005.

881 Honjo, S., and Doherty, K. W.: Large aperture time-series sediment traps; design objectives,
882 construction and application, *Deep Sea Res.*, 35, 133-149, <https://doi.org/10.1016/0198->
883 [0149\(88\)90062-3](https://doi.org/10.1016/0198-0149(88)90062-3), 1988.

884 Hopmans, E. C., Weijers, J. W. H., Schefuß, E., Herfort, L., Sinninghe Damsté, J. S., and
885 Schouten, S.: A novel proxy for terrestrial organic matter in sediments based on branched and isoprenoid
886 tetraether lipids, *Earth Planet. Sc. Lett.*, 224, 107-116, <https://doi.org/10.1016/j.epsl.2004.05.012>, 2004.

887 Hopmans, E. C., Schouten, S., and Sinninghe Damsté, J. S.: The effect of improved
888 chromatography on GDGT-based palaeoproxies, *Org. Geochem.*, 93, 1-6,
889 <http://dx.doi.org/10.1016/j.orggeochem.2015.12.006>, 2016.

890 Huffman, G.J., Adler, R.F., Bolvin, D.T., Gu, G., Nelkin, E.J., Bowman, K.P., Hong, Y.,
891 Stocker, E.F., Wolff, D.B.: The TRMM Multi-satellite Precipitation Analysis: Quasi- Global, Multi-
892 Year, Combined-Sensor Precipitation Estimates at Fine Scale. *J. Hydrometeor.* 8 (1), 38-55,
893 <https://doi.org/10.1175/JHM560.1>, 2007.

894 Hughen, K. A., Overpeck, J. T., Peterson, L. C., and Anderson, R. F.: The nature of varved
895 sedimentation in the Cariaco Basin, Venezuela, and its palaeoclimatic significance, *Geological Society,*
896 *London, Special Publications*, 116, 171-183, <https://doi.org/10.1144/gsl.Sp.1996.116.01.15>, 1996.

897 Hughen, K. A., Overpeck, J. T., Lehman, S. J., Kashgarian, M., Southon, J., Peterson, L. C.,
898 Alley, R., and Sigman, D. M.: Deglacial changes in ocean circulation from an extended radiocarbon
899 calibration, *Nature*, 391, 65-68, <https://doi.org/10.1038/34150>, 1998.

900 Huguet, C., Hopmans, E. C., Febo-Ayala, W., Thompson, D. H., Sinninghe Damsté, J. S., and
901 Schouten, S.: An improved method to determine the absolute abundance of glycerol dibiphytanyl
902 glycerol tetraether lipids, *Org. Geochem.*, 37, 1036-1041,
903 <https://doi.org/10.1016/j.orggeochem.2006.05.008>2006.

904 Huguet, C., Schimmelmann, A., Thunell, R., Lourens, L. J., Sinninghe Damsté, J. S., and
905 Schouten, S.: A study of the TEX₈₆ paleothermometer in the water column and sediments of the Santa
906 Barbara Basin, California, *Paleoceanography*, 22, <https://doi.org/10.1029/2006pa001310>, 2007.

907 Jiang, S., O'Leary, T., Volkman, J. K., Zhang, H., Jia, R., Yu, S., Wang, Y., Luan, Z., Sun, Z.,
908 and Jiang, R.: Origins and simulated thermal alteration of sterols and keto-alcohols in deep-sea marine-
909 sediments of the Okinawa Trough, *Org. Geochem.*, 21, 415-422, <https://doi.org/10.1016/0146->
910 6380(94)90203-8, 1994.

911 Jonas, A. S., Schwark, L., and Bauersachs, T.: Late Quaternary water temperature variations of
912 the Northwest Pacific based on the lipid paleothermometers TEX₈₆^H, U^K₃₇ and LDI, *Deep-Sea Res. Pt.*
913 *I*, 125, 81-93, <http://doi.org/10.1016/j.dsr.2017.04.018>, 2017.

914 Karner, M. B., DeLong, E. F., and Karl, D. M.: Archaeal dominance in the mesopelagic zone
915 of the Pacific Ocean, *Nature*, 409, 507-510, <https://doi.org/10.1038/35054051>, 2001.

916 Kim, J.-H., Schouten, S., Hopmans, E. C., Donner, B., and Sinninghe Damsté, J. S.: Global
917 sediment core-top calibration of the TEX₈₆ paleothermometer in the ocean, *Geochim. Cosmochim. Ac.*,
918 72, 1154-1173, <https://doi.org/10.1016/j.gca.2007.12.010>, 2008.

919 Kim, J.-H., van der Meer, J., Schouten, S., Helmke, P., Willmott, V., Sangiorgi, F., Koc, N.,
920 Hopmans, E. C., and Sinninghe Damsté, J. S.: New indices and calibrations derived from the distribution
921 of crenarchaeal isoprenoid tetraether lipids: Implications for past sea surface temperature
922 reconstructions, *Geochim. Cosmochim. Ac.*, 74, 4639-4654, <https://doi.org/10.1016/j.gca.2010.05.027>,
923 2010.

924 Kim, J.-H., Romero, O. E., Lohmann, G., Donner, B., Laepple, T., Haam, E., and Sinninghe
925 Damsté, J. S.: Pronounced subsurface cooling of North Atlantic waters off Northwest Africa during
926 Dansgaard–Oeschger interstadials, *Earth Planet. Sc. Lett.*, 339-340, 95-102,
927 <https://doi.org/10.1016/j.epsl.2012.05.018>, 2012.

928 Kim, J.-H., Schouten, S., Rodrigo-Gámiz, M., Rampen, S., Marino, G., Huguet, C., Helmke, P.,
929 Buscail, R., Hopmans, E. C., Pross, J., Sangiorgi, F., Middelburg, J. B. M., and Sinninghe Damsté, J.
930 S.: Influence of deep-water derived isoprenoid tetraether lipids on the TEX₈₆^H paleothermometer in the
931 Mediterranean Sea, *Geochim. Cosmochim. Ac.*, 150, 125-141,
932 <https://doi.org/10.1016/j.gca.2014.11.017>, 2015.

933 Koning, E., van Iperen, J. M., van Raaphorst, W., Helder, W., Brummer, G.-J. A., and van
934 Weering, T. C. E.: Selective preservation of upwelling-indicating diatoms in sediments off Somalia,
935 NW Indian Ocean, *Deep-Sea Res. Pt. I*, 48, 2473-2495, [https://doi.org/10.1016/S0967-0637\(01\)00019-](https://doi.org/10.1016/S0967-0637(01)00019-)
936 X, 2001.

937 Korte, L. F., Brummer, G. J. A., van der Does, M., Guerreiro, C. V., Hennekam, R., van Hateren,
938 J. A., Jong, D., Munday, C. I., Schouten, S., and Stuut, J. B. W.: Downward particle fluxes of biogenic
939 matter and Saharan dust across the equatorial North Atlantic, *Atmos. Chem. Phys.*, 17, 6023-6040,
940 <https://doi.org/10.5194/acp-17-6023-2017>, 2017.

941 Lange, C. B., Romero, O. E., Wefer, G., and Gabric, A. J.: Offshore influence of coastal
942 upwelling off Mauritania, NW Africa, as recorded by diatoms in sediment traps at 2195 m water depth,
943 *Deep-Sea Res. Pt. I*, 45, 986-1013, [https://doi.org/10.1016/s0967-0637\(97\)00103-9](https://doi.org/10.1016/s0967-0637(97)00103-9) 1998.

944 Lattaud, J., Kim, J.-H., De Jonge, C., Zell, C., Sinninghe Damsté, J. S., and Schouten, S.: The
945 C₃₂ alkane-1,15-diol as a tracer for riverine input in coastal seas, *Geochim. Cosmochim. Ac.*, 202, 146-
946 158, <http://doi.org/10.1016/j.gca.2016.12.030>, 2017a.

947 Lattaud, J., Dorhout, D., Schulz, H., Castañeda, I. S., Schefuß, E., Sinninghe Damsté, J. S., and
948 Schouten, S.: The C₃₂ alkane-1,15-diol as a proxy of late Quaternary riverine input in coastal margins,
949 *Clim. Past*, 13, 1049-1061, <http://doi.org/10.5194/cp-13-1049-2017>, 2017b.

950 Lee, T., Lagerloef, G., Gierach, M.M., Kao, H.-Y., Yueh, S., Dohan, K.: Aquarius reveals
951 salinity structure of tropical instability waves, *Geophys. Res. Lett.*, 39, L12610,
952 <https://doi.org/10.1029/2012GL052232>, 2012.

953 Lefèvre, N., Moore, G., Aiken, J., Watson, A., and Cooper, D.: Variability of pCO₂ in the
954 tropical Atlantic in 1995, *J. Geophys. Res.*, C3, 5623-5634, <https://doi.org/10.1029/97JC023031998>.

955 Ljung, G. M., & Box, G. E.: On a measure of lack of fit in time series models. *Biometrika*,
956 65(2), 297-303, <https://www.jstor.org/stable/2335207>, 1978.

957 Locarnini R. A., Mishonov A. V., Antonov J. I., Boyer T. P., Garcia H. E., Baranova O. K.,
958 Zweng M. M., Paver C. R., Reagan J. R., Johnson D. R., Hamilton M., Seidov D.: World Ocean Atlas
959 2013, Volume 1: temperature. Levitus S, Ed.; Mishonov A, Technical Ed.; NOAA Atlas NESDIS 73,
960 40 pp, 2013.

961 Lopes dos Santos, R. A., Prange, M., Castañeda, I. S., Schefuß, E., Mulitza, S., Schulz, M.,
962 Niedermeyer, E. M., Sinninghe Damsté, J. S., and Schouten, S.: Glacial-interglacial variability in
963 Atlantic meridional overturning circulation and thermocline adjustments in the tropical North Atlantic,
964 *Earth Planet. Sc. Lett.*, 300, 407-414, <https://doi.org/10.1016/j.epsl.2010.10.030>, 2010.

965 Lopes dos Santos, R. A. L., Spooner, M. I., Barrows, T. T., De Deckker, P., Sinninghe Damsté,
966 J. S., and Schouten, S.: Comparison of organic (U^K₃₇, TEX₈₆^H, LDI) and faunal proxies (foraminiferal
967 assemblages) for reconstruction of late Quaternary sea surface temperature variability from offshore
968 southeastern Australia, *Paleoceanography*, 28, 377-387, <https://doi.org/10.1002/palo.20035>, 2013.

969 Lutjeharms, J. R. E.: *The Agulhas Current*, 330 pp., Springer, Berlin, 2006.

970 Malauene, B. S., Shillington, F. A., Roberts, M. J., and Moloney, C. L.: Cool, elevated
971 chlorophyll-a waters off northern Mozambique, *Deep-Sea Res. Pt. II*, 100, 68-78,
972 <https://doi.org/10.1016/j.dsr2.2013.10.017>, 2014.

973 Marlowe, I. T., Green, J. C., Neal, A. C., Brassell, S. C., Eglinton, G., and Course, P. A.: Long-
974 Chain ($n\text{-C}_{37}\text{--C}_{39}$) alkenones in the Prymnesiophyceae. Distribution of alkenones and other lipids and
975 their taxonomic significance, *Brit. Phycol. J.*, 19, 203-216,
976 <https://doi.org/10.1080/00071618400650221>, 1984.

977 Martin, J. H., and Fitzwater, S. E.: Iron-deficiency limits phytoplankton growth in the Northeast
978 Pacific Subarctic, *Nature*, 331, 341-343, <https://doi.org/10.1038/331341a0>, 1988.

979 Mazeika, P. A.: Thermal domes in the Eastern Tropical Atlantic Ocean. *Limnol. Oceanogr.*, 12,
980 537-539, <https://doi.org/10.4319/lo.1967.12.3.0537>, 1967.

981 Méjanelle, L., Sanchez-Gargallo, A., Bentaleb, I., and Grimalt, J. O.: Long chain n -alkyl diols,
982 hydroxy ketones and sterols in a marine eustigmatophyte, *Nannochloropsis gaditana*, and in *Brachionus*
983 *plicatilis* feeding on the algae, *Org. Geochem.*, 34, 527-538, Pii s0146-6380(02)00246-2,
984 [https://doi.org/10.1016/s0146-6380\(02\)00246-2](https://doi.org/10.1016/s0146-6380(02)00246-2), 2003.

985 Müller-Karger, F. E., McClain, C. R., and Richardson, P. L.: The dispersal of the Amazon's
986 water, *Nature*, 333, 56-59, <https://doi.org/10.1038/333056a0> 1988.

987 Müller-Karger, F. E., Richardson, P. L., and McGillicuddy, D.: On the offshore dispersal of the
988 Amazon's Plume in the North Atlantic: Comments on the paper by A. Longhurst, "Seasonal cooling and
989 blooming in tropical oceans", *Deep-Sea Res. Pt. I*, 42, 2127-2137, [https://doi.org/10.1016/0967-](https://doi.org/10.1016/0967-0637(95)00085-2)
990 [0637\(95\)00085-2](https://doi.org/10.1016/0967-0637(95)00085-2), 1995.

991 Müller-Karger, F., Varela, R., Thunell, R., Scranton, M., Bohrer, R., Taylor, G., Capelo, J.,
992 Astor, Y., Tappa, E., Ho, T. Y., and Walsh, J. J.: Annual cycle of primary production in the Cariaco
993 Basin: Response to upwelling and implications for vertical export, *J. Geophys. Res.*, 106, 4527-4542,
994 <https://doi.org/10.1029/1999JC000291>, 2001.

995 Müller-Karger, F., Varela, R., Thunell, R., Astor, Y., Zhang, H. Y., Luerssen, R., and Hu, C.
996 M.: Processes of coastal upwelling and carbon flux in the Cariaco Basin, *Deep-Sea Res. Pt. II*, 51, 927-
997 943, <https://doi.org/10.1016/j.dsr2.2003.10.010>, 2004.

998 Müller, P. J., Kirst, G., Ruhland, G., von Storch, I., and Rosell-Melé, A.: Calibration of the
999 alkenone paleotemperature index $U^{K'}_{37}$ based on core-tops from the eastern South Atlantic and the global
1000 ocean (60°N - 60°S), *Geochim. Cosmochim. Ac.*, 62, 1757-1772, [https://doi.org/10.1016/s0016-](https://doi.org/10.1016/s0016-7037(98)00097-0)
1001 [7037\(98\)00097-0](https://doi.org/10.1016/s0016-7037(98)00097-0), 1998.

1002 Müller, P. J., and Fischer, G.: A 4-year sediment trap record of alkenones from the filamentous
1003 upwelling region off Cape Blanc, NW Africa and a comparison with distributions in underlying
1004 sediments, *Deep-Sea Res. Pt. I*, 48, 1877-1903, [https://doi.org/10.1016/S0967-0637\(00\)00109-6](https://doi.org/10.1016/S0967-0637(00)00109-6), 2001.

1005 Naafs, B. D. A., Hefter, J., and Stein, R.: Application of the long chain diol index (LDI)
1006 paleothermometer to the early Pleistocene (MIS 96), *Org. Geochem.*, 49, 83-85,
1007 <http://doi.org/10.1016/j.orggeochem.2012.05.011>, 2012.

1008 NASA Aquarius project: Aquarius Official Release Level 3 Sea Surface Salinity Standard
1009 Mapped Image Daily Data V4.0. Ver. 4.0. PO.DAAC, CA, USA, 2015a.

1010 NASA Aquarius project: Aquarius Official Release Level 3 Wind Speed Standard Mapped
1011 Image Daily Data V4.0. Ver. 4.0. PO.DAAC, CA, USA, 2015b.

1012 Nehring, D., Hagen, E., Jorge da Silva, A., Schemainda, R., Wolf, G., Michelchen, N., Kaiser,
1013 W., Postel, L., Gosselk, F., and Brenning, U.: The oceanological conditions in the western part of the
1014 Mozambique Channel in February-March 1980, 1984.

1015 Peeters, F. J. C., Acheson, R., Brummer, G. J. A., de Ruijter, W. P. M., Schneider, R. R.,
1016 Ganssen, G. M., Ufkes, E., and Kroon, D.: Vigorous exchange between the Indian and Atlantic oceans
1017 at the end of the past five glacial periods, *Nature*, 430, 661-665, <http://doi.org/10.1038/nature02785>,
1018 2004.

1019 Peterson, L. C., Overpeck, J. T., Kipp, N. G., and Imbrie, J.: A high-resolution Late Quaternary
1020 upwelling record from the anoxic Cariaco Basin, Venezuela, *Paleoceanography*, 6, 99-119,
1021 <http://doi.org/10.1029/90pa02497>, 1991.

1022 Prah, F. G., and Wakeham, S. G.: Calibration of unsaturation patterns in long-chain ketone
1023 compositions for paleotemperature assessment, *Nature*, 330, 367-369, <http://doi.org/10.1038/330367a0>,
1024 1987.

1025 Prah, F. G., Dymond, J., and Sparrow, M. A.: Annual biomarker record for export production
1026 in the central Arabian Sea, *Deep-Sea Res. II*, 47, 1581-1604, [https://doi.org/10.1016/S0967-](https://doi.org/10.1016/S0967-0645(99)00155-1)
1027 [0645\(99\)00155-1](https://doi.org/10.1016/S0967-0645(99)00155-1), 2000.

1028 Rampen, S. W., Schouten, S., Wakeham, S. G., and Sinninghe Damsté, J. S.: Seasonal and
1029 spatial variation in the sources and fluxes of long chain diols and mid-chain hydroxy methyl alkanooates
1030 in the Arabian Sea, *Org. Geochem.*, 38, 165-179, <https://doi.org/10.1016/j.orggeochem.2006.10.008>,
1031 2007.

1032 Rampen, S. W., Schouten, S., Koning, E., Brummer, G.-J. A., and Sinninghe Damsté, J. S.: A
1033 90 kyr upwelling record from the northwestern Indian Ocean using a novel long-chain diol index, *Earth*
1034 *Planet. Sc. Lett.*, 276, 207-213, <https://doi.org/10.1016/j.epsl.2008.09.022>2008.

1035 Rampen, S. W., Schouten, S., and Sinninghe Damsté, J. S.: Occurrence of long chain 1,14-diols
1036 in *Apedinella radians*, *Org. Geochem.*, 42, 572-574, <https://doi.org/10.1016/j.orggeochem.2011.03.009>,
1037 2011.

1038 Rampen, S. W., Willmott, V., Kim, J. H., Uliana, E., Mollenhauer, G., Schefuss, E., Sinninghe
1039 Damsté, J. S., and Schouten, S.: Long chain 1,13-and 1,15-diols as a potential proxy for
1040 palaeotemperature reconstruction, *Geochim. Cosmochim. Ac.*, 84, 204-216,
1041 <https://doi.org/10.1016/j.gca.2012.01.024>, 2012.

1042 Rampen, S. W., Willmott, V., Kim, J. H., Rodrigo-Gámiz, M., Uliana, E., Mollenhauer, G.,
1043 Schefuss, E., Sinninghe Damsté, J. S., and Schouten, S.: Evaluation of long chain 1,14-alkyl diols in
1044 marine sediments as indicators for upwelling and temperature, *Org. Geochem.*, 76, 39-47,
1045 <https://doi.org/10.1016/j.orggeochem.2014.07.012>, 2014a.

1046 Rampen, S. W., Datema, M., Rodrigo-Gámiz, M., Schouten, S., Reichart, G. J., and Sinninghe
1047 Damsté, J. S.: Sources and proxy potential of long chain alkyl diols in lacustrine environments,
1048 *Geochim. Cosmochim. Ac.*, 144, 59-71, <https://doi.org/10.1016/j.gca.2014.08.033>, 2014b.

1049 Reiche, S., Rampen, S. W., Dorhout, D. J. C., Sinninghe Damsté, J. S., and Schouten, S.: The
1050 impact of oxygen exposure on long-chain alkyl diols and the long chain diol index (LDI) – a long-term
1051 incubation study, *Org. Geochem.*, 124, 238-246, <https://doi.org/10.1016/j.orggeochem.2018.08.003>,
1052 2018.

1053 Richards, F. A. 1975. The Cariaco Basin (Trench). *Oceanogr. Mar. Biol. Ann. Rev.* 13: 11–67.

1054 Richardson, P. L., and Reverdin, G.: Seasonal cycle of velocity in the Atlantic North Equatorial
1055 Countercurrent as measured by surface drifters, current meters, and ship drifts, *J. Geophys. Res.-Oceans*,
1056 92, 3691-3708, <https://doi.org/10.1029/JC092iC04p03691>, 1987.

1057 Ridderinkhof, H., van der Werf, P. M., Ullgren, J. E., van Aken, H. M., van Leeuwen, P. J., and
1058 de Ruijter, W. P. M.: Seasonal and interannual variability in the Mozambique Channel from moored
1059 current observations, *J. Geophys. Res.-Oceans*, 115, <https://doi.org/10.1029/2009jc005619>, 2010.

1060 Rodrigo-Gámiz, M., Rampen, S. W., de Haas, H., Baas, M., Schouten, S., and Sinninghe
1061 Damsté, J. S.: Constraints on the applicability of the organic temperature proxies $U^{K'_{37}}$, TEX_{86} and LDI
1062 in the subpolar region around Iceland, *Biogeosciences*, 12, 6573-6590, <https://doi.org/10.5194/bg-12-6573-2015>, 2015.

1064 Rodrigo-Gámiz, M., Rampen, S. W., Schouten, S., and Sinninghe Damsté, J. S.: The impact of
1065 oxic degradation on long chain alkyl diol distributions in Arabian Sea surface sediments, *Org.*
1066 *Geochem.*, 100, 1-9, <http://doi.org/10.1016/j.orggeochem.2016.07.003>, 2016.

1067 Romero O. E., Lange C. B., Fischer G., Treppke U. F., Wefer G.: Variability in Export
1068 Production Documented by Downward Fluxes and Species Composition of Marine Planktic Diatoms:
1069 Observations from the Tropical and Equatorial Atlantic. In: Fischer G., Wefer G. (eds) Use of Proxies
1070 in Paleoceanography. Springer, Berlin, Heidelberg, 1999.

1071 Rosell-Melé, A., and Prahl, F. G.: Seasonality of $U^{K_{37}}$ temperature estimates as inferred from
1072 sediment trap data, Quaternary Sci. Rev., 72, 128-136, <https://doi.org/10.1016/j.quascirev.2013.04.017>,
1073 2013.

1074 Rossignol, M., and A.M. Meyruis, Campagnes océanographiques du Gérard-Tréca, 53 pp.,
1075 Cent. Oceanogr. Dakar-Thiaroye, ORSTOM, Dakar, Senegal, 1964.

1076 Sætre, R., and Da Silva, A. J.: The circulation of the Mozambique channel, Deep Sea Res., 31,
1077 485-508, [https://doi.org/10.1016/0198-0149\(84\)90098-0](https://doi.org/10.1016/0198-0149(84)90098-0), 1984.

1078 Schlitzer, R.: Data Analysis and Visualization with Ocean Data View, CMOS Bulletin SCMO,
1079 43, 9–13, available at: <https://odv.awi.de/>, 2015.

1080 Schouten, M. W., de Ruijter, W. P. M., van Leeuwen, P. J., and Ridderinkhof, H.: Eddies and
1081 variability in the Mozambique Channel, Deep-Sea Res. Pt. II, 50, 1987-2003,
1082 [https://doi.org/10.1016/s0967-0645\(03\)00042-0](https://doi.org/10.1016/s0967-0645(03)00042-0), 2003.

1083 Schouten, S., Hopmans, E. C., Schefuss, E., and Sinninghe Damsté, J. S.: Distributional
1084 variations in marine crenarchaeotal membrane lipids: a new tool for reconstructing ancient sea water
1085 temperatures?, Earth Planet. Sc. Lett., 204, 265-274, [https://doi.org/10.1016/s0012-821x\(02\)00979-2](https://doi.org/10.1016/s0012-821x(02)00979-2),
1086 2002.

1087 Schouten, S., Hopmans, E. C., and Sinninghe Damsté, J. S.: The organic geochemistry of
1088 glycerol dialkyl glycerol tetraether lipids: A review, Org. Geochem., 54, 19-61,
1089 <https://doi.org/10.1016/j.orggeochem.2012.09.006>, 2013.

1090 Schreuder, L. T., Stuut, J.-B. W., Korte, L. F., Sinninghe Damsté, J. S., and Schouten, S.:
1091 Aeolian transport and deposition of plant wax *n*-alkanes across the tropical North Atlantic Ocean, Org.
1092 Geochem., 115, 113-123, <https://doi.org/10.1016/j.orggeochem.2017.10.010>, 2018a.

1093 Schreuder, L. T., Hopmans, E. C., Stuut, J.-B. W., Sinninghe Damsté, J. S., and Schouten, S.:
1094 Transport and deposition of the fire biomarker levoglucosan across the tropical North Atlantic Ocean,
1095 Geochim. Cosmochim. Ac., 227, 171-185, <https://doi.org/10.1016/j.gca.2018.02.020>, 2018b.

1096 Siedler, G., Zangenberg, N., and Onken, R.: Seasonal Changes in the Tropical Atlantic
1097 Circulation – Observation and Simulation of the Guinea Dome, J. Geophys. Res.-Oceans, 97, 703-715,
1098 <https://doi.org/10.1029/91jc02501>, 1992.

1099 Sinninghe Damsté, J. S., Rijpstra, W. I. C., Hopmans, E. C., Prahl, F. G., Wakeham, S. G., and
1100 Schouten, S.: Distribution of membrane lipids of planktonic Crenarchaeota in the Arabian sea, *App.*
1101 *Environ. Micr.*, 68, 2997-3002, <https://doi.org/10.1128/aem.68.6.2997-3002.2002>, 2002.

1102 Sinninghe Damsté, J. S., Rijpstra, W. I. C., and Reichart, G.-J.: The influence of oxic
1103 degradation on the sedimentary biomarker record II. Evidence from Arabian Sea sediments, *Geochim.*
1104 *Cosmochim. Ac.*, 66, 2737-2754, [https://doi.org/10.1016/S0016-7037\(02\)00865-7](https://doi.org/10.1016/S0016-7037(02)00865-7), 2002.

1105 Sinninghe Damsté, J. S., Rampen, S., Rijpstra, W. I. C., Abbas, B., Muyzer, G., and Schouten,
1106 S.: A diatomaceous origin for long-chain diols and mid-chain hydroxy methyl alkanooates widely
1107 occurring in Quaternary marine sediments: Indicators for high-nutrient conditions, *Geochim.*
1108 *Cosmochim. Ac.*, 67, 1339-1348, [https://doi.org/10.1016/s0016-7037\(02\)01225-5](https://doi.org/10.1016/s0016-7037(02)01225-5) 2003.

1109 Sinninghe Damsté, J. S., Rijpstra, W. I. C., Hopmans, E. C., den Uijl, M. J., Weijers, J. W. H.,
1110 and Schouten, S.: The enigmatic structure of the crenarchaeol isomer, *Org. Geochem.*, 124, 22-28,
1111 <https://doi.org/10.1016/j.orggeochem.2018.06.005>, 2018.

1112 Smith, S. L.: Understanding the Arabian Sea: Reflections on the 1994-1996 Arabian Sea
1113 Expedition, *Deep-Sea Res. Pt. II*, 48, 1385-1402, [https://doi.org/10.1016/S0967-0645\(00\)00144-2](https://doi.org/10.1016/S0967-0645(00)00144-2),
1114 2001.

1115 Stramma, L., and Schott, F.: The mean flow field of the tropical Atlantic Ocean, *Deep-Sea Res.*
1116 *Pt. II*, 46, 279-303, [https://doi.org/10.1016/s0967-0645\(98\)00109-x](https://doi.org/10.1016/s0967-0645(98)00109-x), 1999.

1117 Stuut, J.-B., Zabel, M., Ratmeyer, V., Helmke, P., Schefuß, E., Lavik, G., and Schneider, R.:
1118 Provenance of present-day eolian dust collected off NW Africa, *J. Geophys. Res.-Atmos.*, 110, D04202-
1119 04201-D04202-04214, <https://doi.org/10.1029/2004JD005161>, 2005.

1120 Thunell, R. C., Varela, R., Llano, M., Collister, J., Müller-Karger, F., and Bohrer, R.: Organic
1121 carbon fluxes, degradation, and accumulation in an anoxic basin: Sediment trap results from the Cariaco
1122 Basin, *Limnol. Oceanogr.*, 45, 300-308, <https://doi.org/10.4319/lo.2000.45.2.0300>, 2000.

1123 Thunell, R., Benitez-Nelson, C., Varela, R., Astor, Y., and Müller-Karger, F.: Particulate
1124 organic carbon fluxes along upwelling-dominated continental margins: Rates and mechanisms, *Global*
1125 *Biogeochem. Cy.*, 21, <https://doi.org/10.1029/2006gb002793>, 2007.

1126 Tierney, J. E.: 12.14 - Biomarker-Based Inferences of Past Climate: The TEX₈₆
1127 Paleotemperature Proxy A2 - Holland, Heinrich D, in: *Treatise on Geochemistry (Second Edition)*,
1128 edited by: Turekian, K. K., Elsevier, Oxford, 379-393, 2014.

1129 Tierney, J. E., and Tingley, M. P.: A Bayesian, spatially-varying calibration model for the TEX₈₆
1130 proxy, *Geochim. Cosmochim. Ac.*, 127, 83-106, <https://doi.org/10.1016/j.gca.2013.11.026>, 2014.

1131 Tierney, J. E., and Tingley, M. P.: A TEX₈₆ surface sediment database and extended Bayesian
1132 calibration, *Scientific Data*, 2, 150029, <https://doi.org/10.1038/sdata.2015.29>, 2015.

1133 Tierney, J. E., Sinninghe Damsté, J. S., Pancost, R. D., Sluijs, A., and Zachos, J. C.: Eocene
1134 temperature gradients, *Nature Geosci*, 10, 538-539, <https://doi.org/10.1038/ngeo2997>, 2017

1135 Tierney, J. E., and Tingley, M. P.: BAYSPLINE: A New Calibration for the Alkenone
1136 Paleothermometer, *Paleoceanography and Paleoclimatology*, 33, 281-301,
1137 <https://doi.org/10.1002/2017pa003201>, 2018.

1138 Torrence, C., Compo, G. P.: A practical guide to wavelet analysis. *Bull. Am. Meteorol. Soc.* 79,
1139 61–78, [https://doi.org/10.1175/1520-0477\(1998\)079<0061:APGTWA>2.0.CO;2](https://doi.org/10.1175/1520-0477(1998)079<0061:APGTWA>2.0.CO;2), 1998.

1140 Treppke, U. F., Lange, C. B., and Wefer, G.: Vertical fluxes of diatoms and silicoflagellates in
1141 the eastern equatorial Atlantic, and their contribution to the sedimentary record, *Mar. Micropaleontol.*,
1142 28, 73-96, [https://doi.org/10.1016/0377-8398\(95\)00046-1](https://doi.org/10.1016/0377-8398(95)00046-1), 1996.

1143 Turich, C., Schouten, S., Thunell, R. C., Varela, R., Astor, Y., and Wakeham, S. G.: Comparison
1144 of TEX₈₆ and U^K₃₇ temperature proxies in sinking particles in the Cariaco Basin, *Deep-Sea Res. Pt. I*,
1145 78, 115-133, <http://doi.org/10.1016/j.dsr.2013.02.008>, 2013.

1146 Ullgren, J. E., van Aken, H. M., Ridderinkhof, H. and de Ruijter, W. P. M.: The hydrography
1147 of the Mozambique Channel from six years of continuous temperature, salinity, and velocity
1148 observations. *Deep-Sea Res. Pt. I*, 69, 36 – 50, <https://doi.org/10.1016/j.dsr.2012.07.003>, 2012.

1149 Villanueva, L., Besseling, M., Rodrigo-Gámiz, M., Rampen, S. W., Verschuren, D., and
1150 Sinninghe Damsté, J. S.: Potential biological sources of long chain alkyl diols in a lacustrine system,
1151 *Org. Geochem.*, 68, 27-30, <https://doi.org/10.1016/j.orggeochem.2014.01.001>, 2014.

1152 van der Does, M., Korte, L. F., Munday, C. I., Brummer, G. J. A., and Stuut, J. B. W.: Particle
1153 size traces modern Saharan dust transport and deposition across the equatorial North Atlantic, *Atmos.*
1154 *Chemis. Phys.*, 16, 13697-13710, <https://doi.org/10.5194/acp-16-13697-2016>, 2016.

1155 Versteegh, G. J. M., Bosch, H. J., and de Leeuw, J. W.: Potential palaeoenvironmental
1156 information of C₂₄ to C₃₆ mid-chain diols, keto-ols and mid-chain hydroxy fatty acids; a critical review,
1157 *Org. Geochem.*, 27, 1-13, [https://doi.org/10.1016/s0146-6380\(97\)00063-6](https://doi.org/10.1016/s0146-6380(97)00063-6), 1997.

1158 Versteegh, G. J. M., Jansen, J. H. F., de Leeuw, J. W., and Schneider, R. R.: Mid-chain diols
1159 and keto-ols in SE Atlantic sediments: a new tool for tracing past sea surface water masses?, *Geochim.*
1160 *Cosmochim. Ac.*, 64, 1879-1892, [https://doi.org/10.1016/S0016-7037\(99\)00398-1](https://doi.org/10.1016/S0016-7037(99)00398-1), 2000.

1161 Voituriez, B.: Les sous-courants équatioriaux nord et sud et la formation des dômes thermiques
1162 tropicaux, *Oceanol. Acta*, 4,497-506, 1981.

1163 Volkman, J. K., Eglinton, G., Corner, E. D. S., and Sargent, J. R.: Novel unsaturated straight-
1164 chain C₃₇-C₃₉ methyl and ethyl ketones in marine sediments and a coccolithophore *Emiliania huxleyi*,
1165 Phys. Chem. Earth, 12, 219-227, [http://doi.org/10.1016/0079-1946\(79\)90106-X](http://doi.org/10.1016/0079-1946(79)90106-X), 1980.

1166 Volkman, J. K., Barrett, S. M., Dunstan, G. A., and Jeffrey, S. W.: C₃₀-C₃₂ alky diols and
1167 unsaturated alcohols in microalgae of the class Eustigmatophyceae, Org. Geochem., 18, 131-138,
1168 [http://doi.org/10.1016/0146-6380\(92\)90150-v](http://doi.org/10.1016/0146-6380(92)90150-v), 1992.

1169 Volkman, J. K., Barrett, S. M., Blackburn, S. I., and Sikes, E. L.: Alkenones in *Gephyrocapsa*
1170 *Oceanica* – Implications for studies of paleoclimate, Geochim. Cosmochim. Ac., 59, 513-520,
1171 [http://doi.org/10.1016/0016-7037\(95\)00325-t](http://doi.org/10.1016/0016-7037(95)00325-t), 1995.

1172 Volkman, J. K., Barrett, S. M., and Blackburn, S. I.: Eustigmatophyte microalgae are potential
1173 sources of C₂₉ sterols, C₂₂-C₂₈ *n*-alcohols and C₂₈-C₃₂ *n*-alkyl diols in freshwater environments, Org.
1174 Geochem., 30, 307-318, [http://doi.org/10.1016/S0146-6380\(99\)00009-1](http://doi.org/10.1016/S0146-6380(99)00009-1), 1999.

1175 Wakeham, S. G., Peterson, M. L., Hedges, J. I., and Lee, C.: Lipid biomarker fluxes in the
1176 Arabian Sea, with a comparison to the equatorial Pacific Ocean, Deep-Sea Res. Pt. II, 49, 2265-2301,
1177 [https://doi.org/10.1016/S0967-0645\(02\)00037-1](https://doi.org/10.1016/S0967-0645(02)00037-1), 2002.

1178 Warnock, J. P., Bauersachs, T., Kotthoff, U., Brandt, H. T., and Andren, E.: Holocene
1179 environmental history of the Angermanalven Estuary, northern Baltic Sea, Boreas, 47, 593-608,
1180 <https://doi.org/10.1111/bor.12281>, 2018.

1181 Weijer, W., de Ruiter, W. P. M., Dijkstra, H. A., and van Leeuwen, P. J.: Impact of interbasin
1182 exchange on the Atlantic overturning circulation, J. Phys. Oceanogr., 29, 2266-2284,
1183 [https://doi.org/10.1175/1520-0485\(1999\)029<2266:Ioieot>2.0.Co;2](https://doi.org/10.1175/1520-0485(1999)029<2266:Ioieot>2.0.Co;2), 1999.

1184 Willmott, V., Rampen, S. W., Domack, E., Canals, M., Sinninghe Damsté, J. S., and Schouten,
1185 S.: Holocene changes in Proboscia diatom productivity in shelf waters of the north-western Antarctic
1186 Peninsula, Antarct. Sci., 22, 3-10, <https://doi.org/10.1017/S095410200999037x>, 2010.

1187 Wuchter, C., Schouten, S., Wakeham, S. G., and Sinninghe Damsté, J. S.: Temporal and spatial
1188 variation in tetraether membrane lipids of marine Crenarchaeota in particulate organic matter:
1189 Implications for TEX₈₆ paleothermometry, Paleoceanography, 20,
1190 <https://doi.org/10.1029/2004pa001110>, 2005.

1191 Wuchter, C., Schouten, S., Wakeham, S. G., and Sinninghe Damsté, J. S.: Archaeal tetraether
1192 membrane lipid fluxes in the northeastern Pacific and the Arabian Sea: Implications for TEX₈₆
1193 paleothermometry, Paleoceanography, 21, PA4208-4201-PA4208-4209,
1194 <https://doi.org/10.1029/2006PA001279>, 2006.

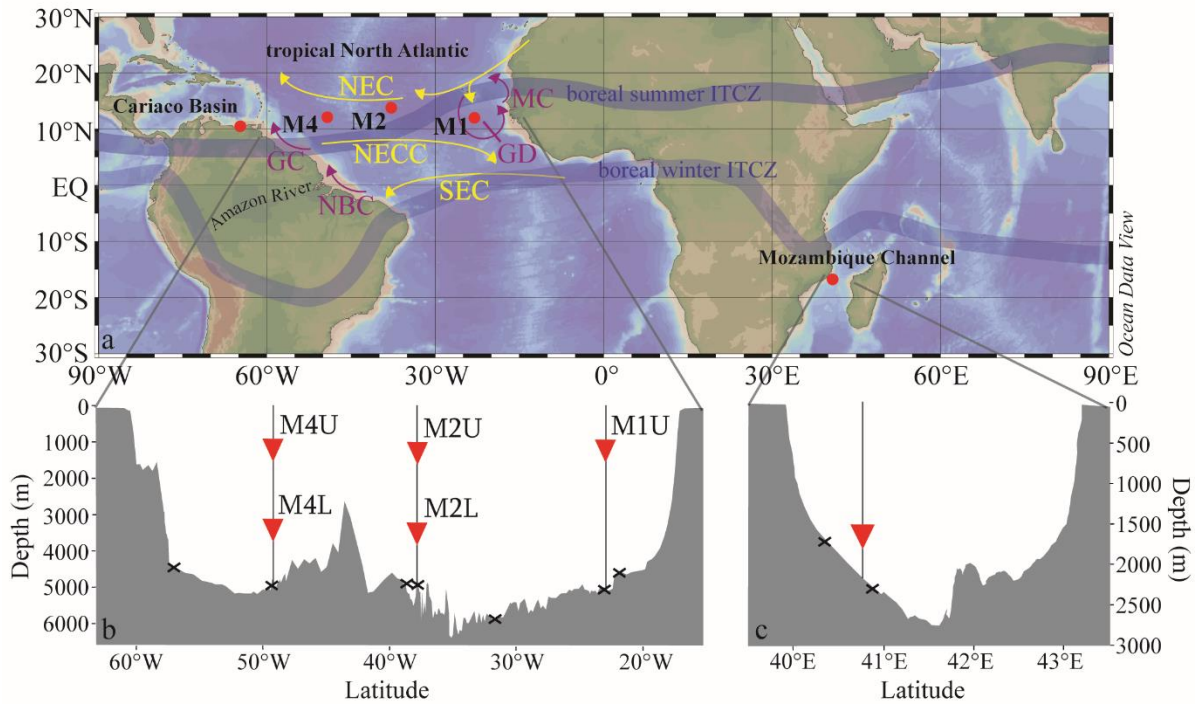
1195 Xie, P. and Arkin, P.A.: Global precipitation: A 17-year monthly analysis based on gauge
1196 observations, satellite estimates, and numerical model outputs. *Bull. Am. Meteor. Soc.*, 78, 2539 – 2558,
1197 [https://doi.org/10.1175/1520-0477\(1997\)078<2539:GPAYMA>2.0.CO;2](https://doi.org/10.1175/1520-0477(1997)078<2539:GPAYMA>2.0.CO;2), 1997.

1198 Yamagata, T., and Iizuka, S.: Simulation of the Tropical Thermal Domes in the Atlantic – A
1199 Seasonal Cycle, *J. Phys. Oceanogr.*, 25, 2129-2140, [https://doi.org/10.1175/1520-0485\(1995\)025<2129:Sotttd>2.0.Co;2](https://doi.org/10.1175/1520-0485(1995)025<2129:Sotttd>2.0.Co;2), 1995.

1201 Yamamoto, M., Shimamoto, A., Fukuhara, T., Tanaka, Y., and Ishizaka, J.: Glycerol dialkyl
1202 glycerol tetraethers and TEX₈₆ index in sinking particles in the western North Pacific, *Org. Geochem.*,
1203 53, 52-62, <https://doi.org/10.1016/j.orggeochem.2012.04.010>, 2012.

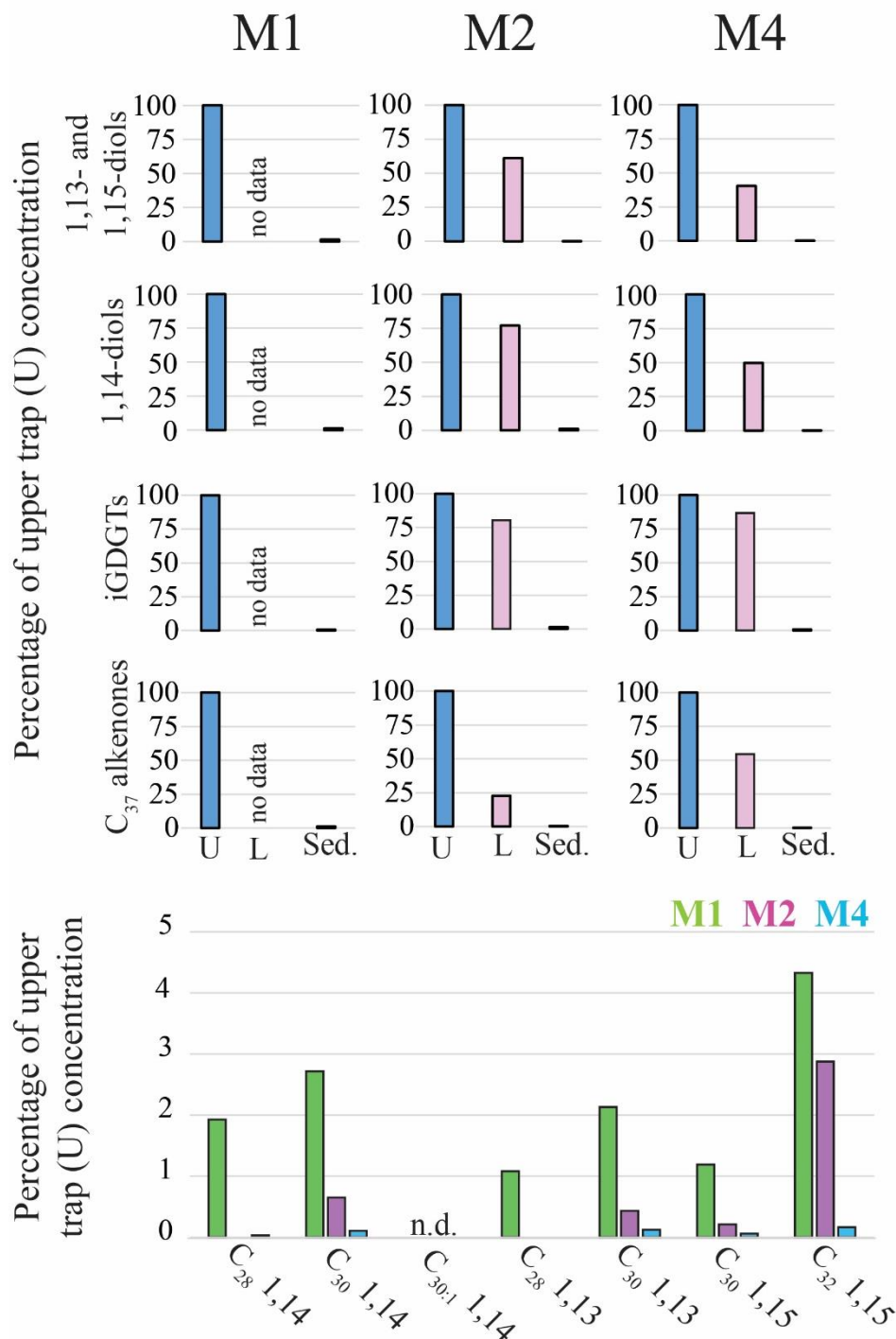
1204 Zhang, Y. G., and Liu, X. Q.: Export Depth of the TEX₈₆ Signal, *Paleoceanography and*
1205 *Paleoclimatology*, 33, 666-671, <https://doi.org/10.1029/2018PA003337>, 2018.

1206



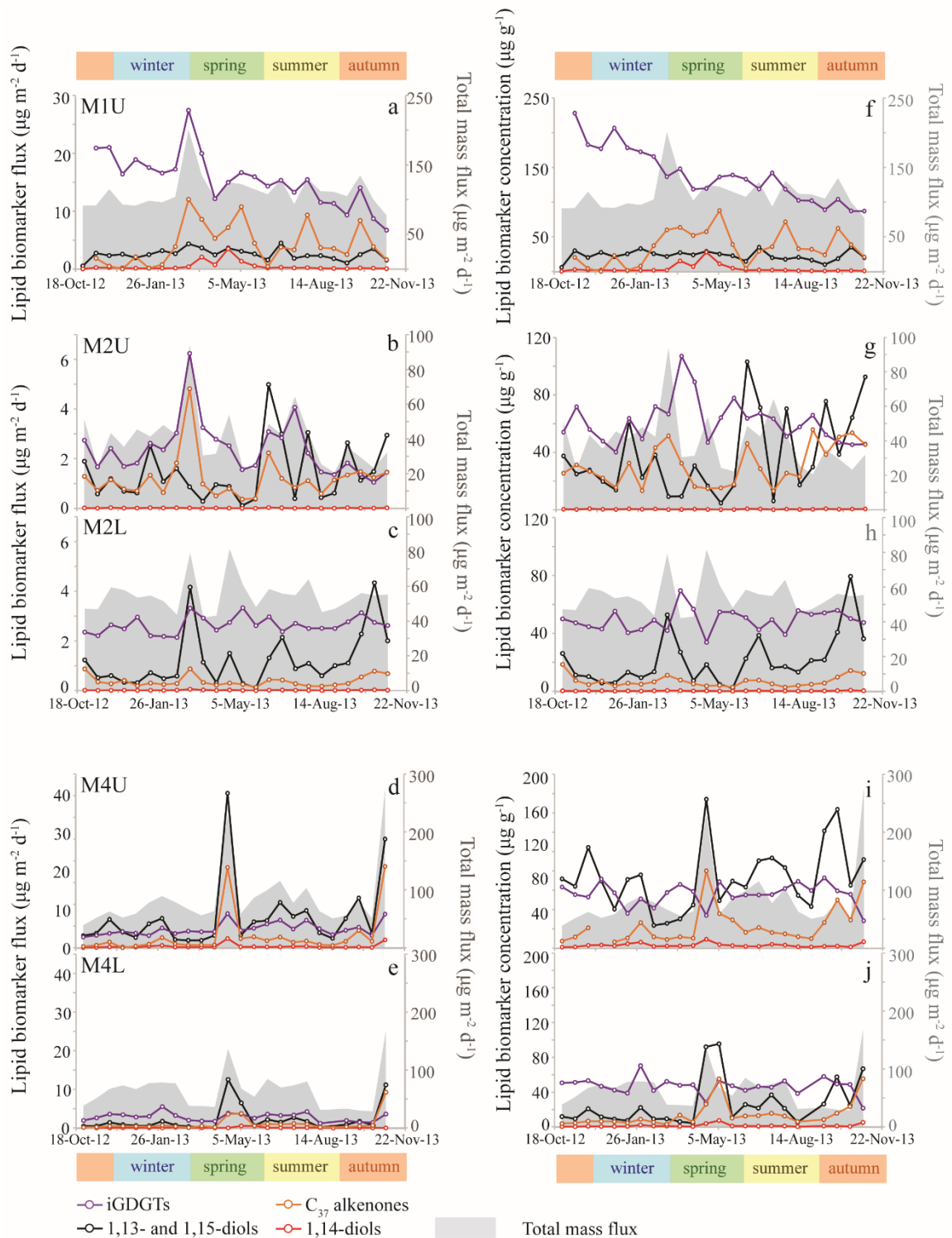
1207

1208 **Fig. 1** (a) Location map showing the five sediment trap mooring sites in the Cariaco Basin, the tropical
 1209 North Atlantic (M1, M2 and M4) and the Mozambique Channel. Two of the moorings in the tropical
 1210 North Atlantic (M2 and M4) contain an upper ('U') and a lower ('L') trap, shown in the bathymetric
 1211 section below (b) with traps depicted as red triangles and surface sediments shown as black crosses. A
 1212 similar section profile is shown for the Mozambique Channel (c), where also the sediment trap and the
 1213 surface sediments are indicated. All maps/sections are generated in Ocean Data View (Schlitzer, 2015).
 1214 Indicated are the approximate seasonal positions of the ITCZ. NEC = North Equatorial Current; NECC
 1215 = North Equatorial Countercurrent; SEC = South Equatorial Current; MC = Mauritania Current; GD =
 1216 Guinea Dome; NBC = North Brazil Current; GC = Guiana Current.

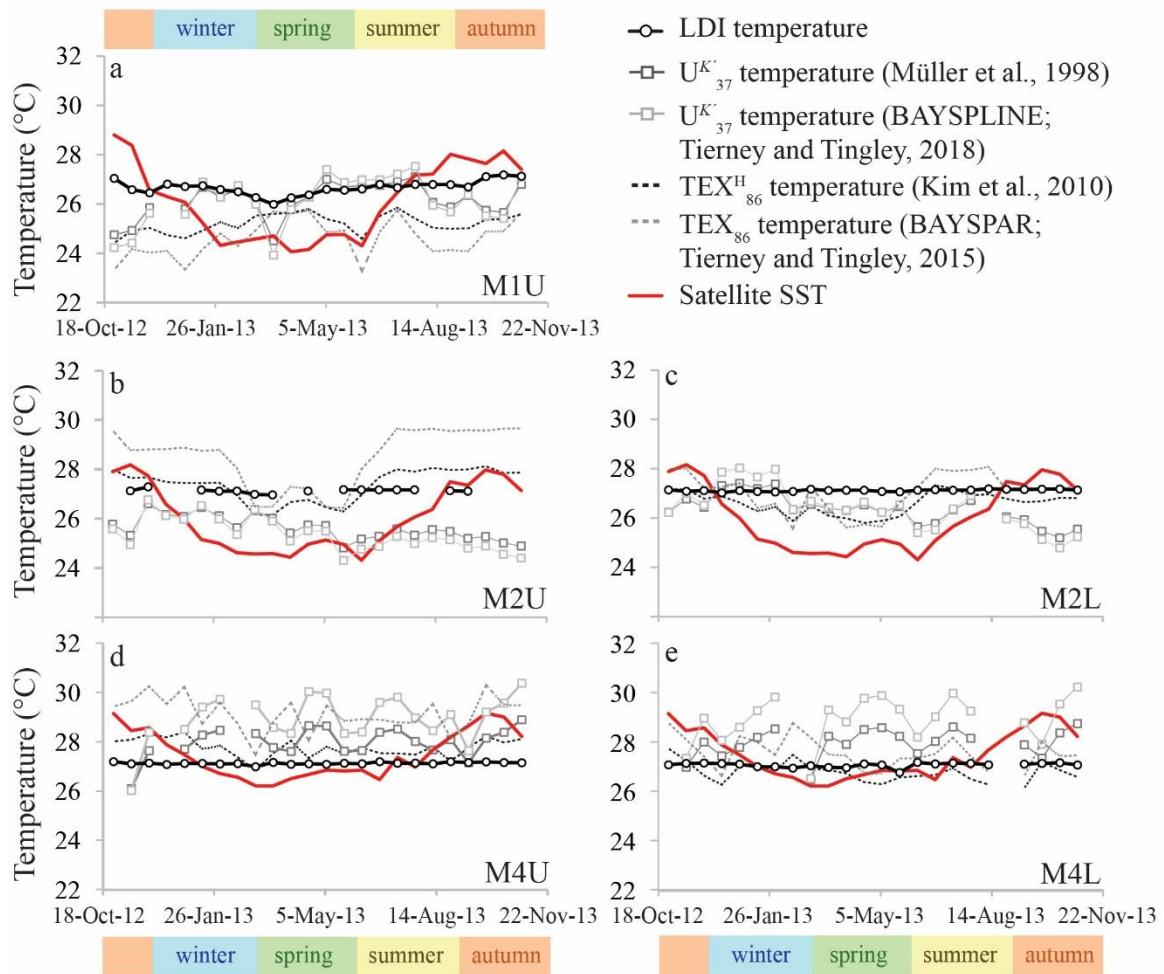


1217

1218 **Fig. 2** Relative concentrations of biomarker lipids for the mooring sites M1, M2 and M4 in the tropical
 1219 North Atlantic. Upper panel: percentages of lipid biomarkers in the lower traps ('L'; 3500 m) and the
 1220 surface sediments ('Sed.') relative to the annual flux-weighted concentrations in the upper traps ('U';
 1221 1200 m; set at 100%). The lower panel shows the preservation of the individual LCDs (sediments versus
 1222 upper trap flux-weighted concentration) for the three sediment trap sites. For M1 and M2 the
 1223 sedimentary LCD concentrations were based on the average of the two nearby underlying surface
 1224 sediments (Fig. 1). When no bar is shown ~~than~~ then the LCD was not detected.



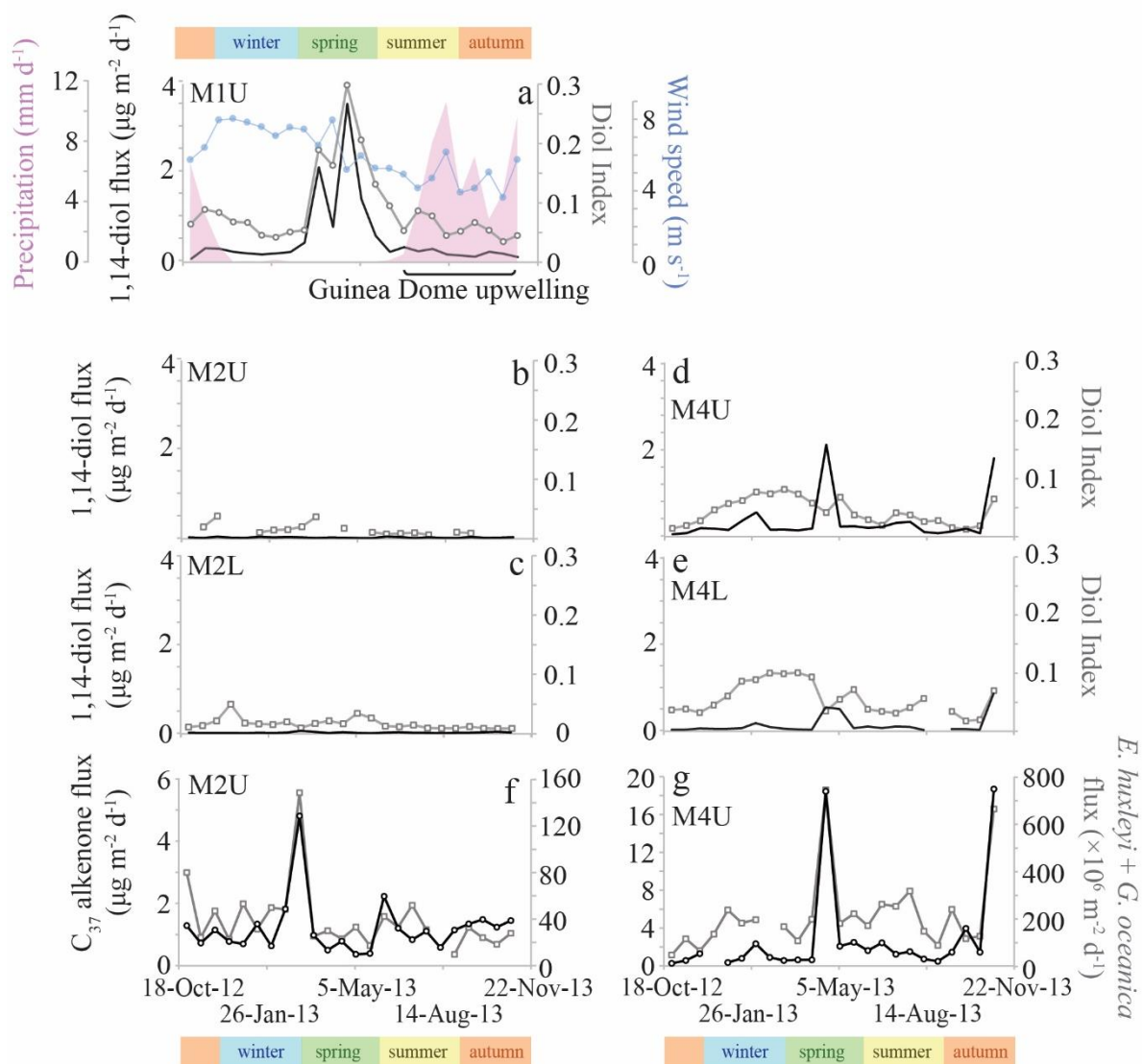
1225 **Fig. 3** Lipid biomarker fluxes for the tropical North Atlantic sediment traps, i.e., M1, upper and lower
 1226 M2, and upper and lower M4 in panels (a) to (e). Lipid biomarker fluxes (iGDGTs in purple; C_{37}
 1227 alkenones in orange; 1,13- and 1,15-diols in black; 1,14-diols in red) are indicated on the left y-axis, and
 1228 the total mass flux (grey stack; Korte et al., 2017) on the right y-axis. Lipid biomarker concentrations
 1229 are plotted in panels (f) to (j), with biomarker concentrations on the left y-axis, and the total mass flux
 1230 on the right y-axis. Note that the y-axes are different per sediment trap site, but identical for upper (U)
 1231 and lower (L) traps.



1232

1233 **Fig. 5-4** Temperature proxy records for the tropical North Atlantic. Panel (a) shows upper trap station
 1234 M1, (b) upper trap station M2 and (c) lower trap M2, respectively, (d) upper trap station M4 and (e)
 1235 lower trap station M4, respectively.

1236



1237

1238 **Fig. 6-5** Phytoplankton productivity records for the tropical North Atlantic. Panels (a) – (e) show the
 1239 1,14-diol fluxes (left y-axis; black) and the Diol Index (right y-axis; grey) for sediment traps. The y-axes
 1240 are the same for these panels. Wind speed and precipitation data were adapted from Guerreiro et al. (in
 1241 revision); for references regarding remote sensing parameters, see Guerreiro et al. (2017). Panels (f) and
 1242 (g) show the C₃₇ alkenone fluxes (left y-axis; black) and combined fluxes of *E. huxleyi* and *G. oceanica*
 1243 (from Guerreiro et al., 2017; right y-axis; grey) for the upper traps of M2 and M4.

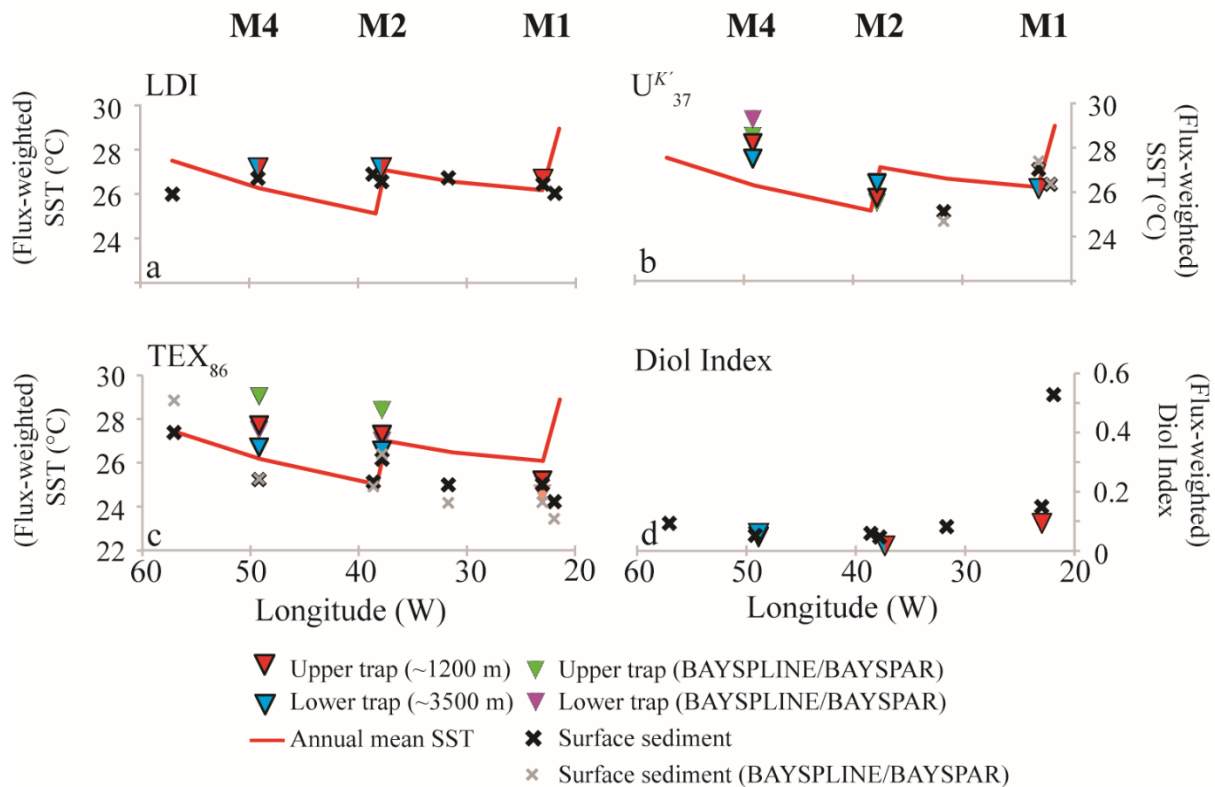
1244

1245

1246

1247

1248



1249

1250

1251

1252

1253

1254

1255

1256

1257

1258

1259

1260

1261

1262

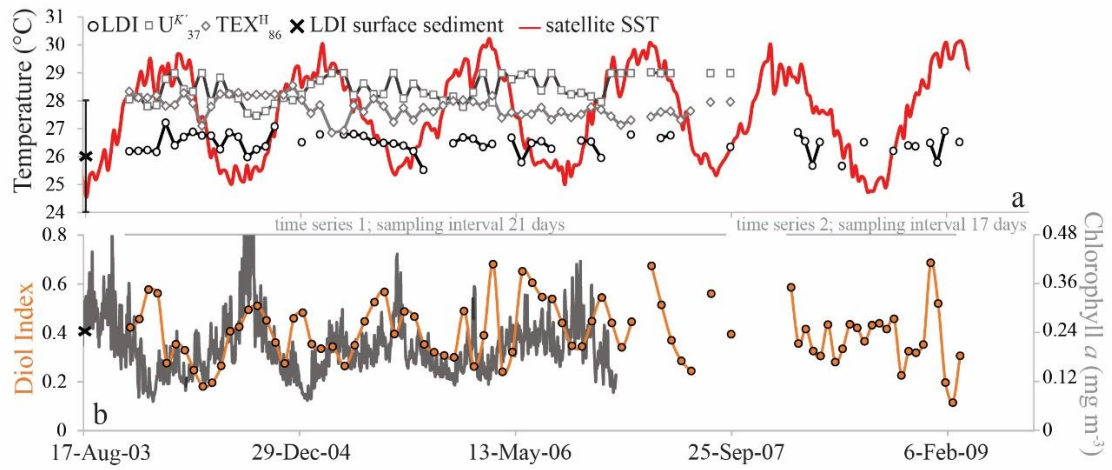
1263

1264

1265

1266

Fig. 7-6 (a) Annual mean temperature profiles at the sediment trap locations (World Ocean Atlas 2013) with approximate proxy lipid production depths indicated, as deduced from Balzano et al. (unpublished results). **(b)** Flux-weighted average (annual) proxy results for the sediment traps compared with the underlying sediments (crosses) and annual mean SST (red line; specific for coordinates of the surface sediments; World Ocean Atlas 2013 ¼ grid resolution~~World Ocean Atlas 2013~~). Panel **(ba)**, **(eb)** and **(dc)** show the LDI, $U^{K'_{37}}$ and TEX_{86} temperature results, respectively. Triangles reflect sediment trap results (red = upper/~1200 m; blue = lower/~3500 m), and crosses represent surface sediments. In case of the $U^{K'_{37}}$ and TEX_{86} , the green and purple triangles and grey crosses reflect the temperatures calculated using the BAYSPLINE and BAYSPAR models (Tierney and Tingley, 2014; 2015; 2018), whereas the other temperatures were calculated by means of the Müller et al. (1998) and Kim et al. (2010; TEX_{86}^H) calibrations, respectively. Panel **(d)** shows the flux-weighted average Diol Index values for the sediment traps, and the Diol Index estimates for the surface sediments.

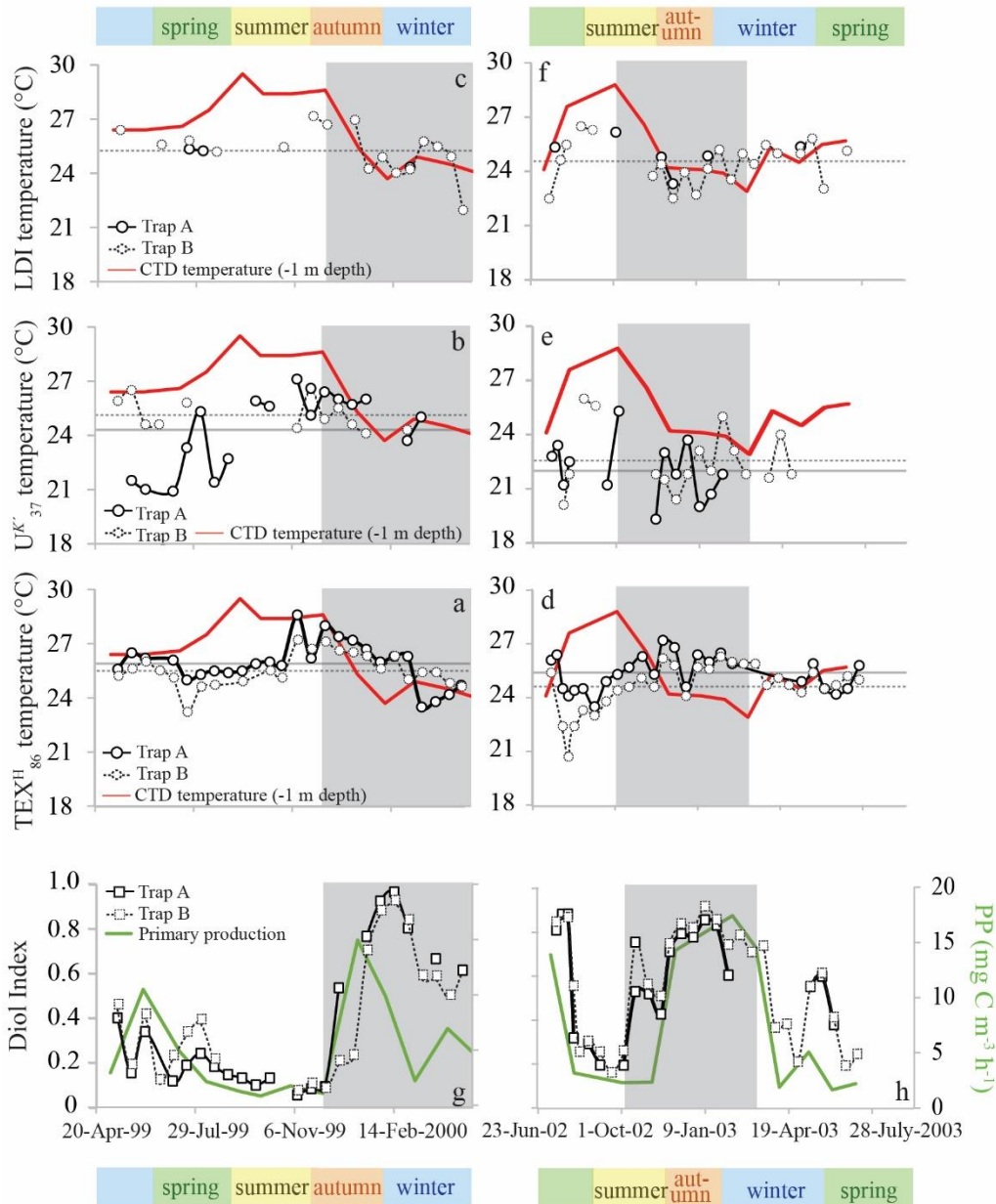


1267

1268 **Fig. 7** The LDI-derived temperatures, together with the $\text{TEX}^{\text{H}}_{86}$ and U^{K}_{37} -derived temperatures
 1269 and satellite SST (Fallet et al., 2011) (a) and the Diol Index (b) for the Mozambique Channel sediment
 1270 trap. The black cross in panel (a) reflects the average LDI temperature of two underlying surface
 1271 sediments, with the LDI calibration error. The chlorophyll *a* data is from Fallet et al. (2011).

1272

1273



1274

1275 **Fig. 8** Seasonal proxy derived temperature and upwelling/productivity records for the sediment
 1276 traps in the Cariaco Basin. Panels (a), (b) and (c) show the May 1999 – May 2000 time series $\text{TEX}^{\text{H}}_{86}$ -,
 1277 $U^{K'}_{37}$ - and LDI-derived temperature reconstructions for Trap A (275 m depth; solid symbols) and Trap
 1278 B (455 m depth; dashed symbols), respectively. Panels (d), (e) and (f) show the proxy data for the July
 1279 2002 – July 2003 time series, with CTD-temperatures (1 m depth) in red. The $U^{K'}_{37}$, $\text{TEX}^{\text{H}}_{86}$ and CTD
 1280 temperatures are adopted from Turich et al. (2013). The horizontal lines reflect the average proxy-
 1281 derived temperatures (Trap A = solid; Trap B = dashed). Panel (g) and (h) show the 1,14-diol based
 1282 Diol Index (Rampen et al., 2008) for the 1999-2000 and 2002-2003 time series, respectively, for Trap
 1283 A (275 m depth; solid symbols) and Trap B (455 m depth; dashed symbols). Primary productivity in mg
 1284 $\text{C m}^{-3} \text{h}^{-1}$ is plotted in green (data adopted from Turich et al., 2013). The shaded area reflects the period
 1285 of upwelling.

1286
1287
1288
1289
1290
1291
1292
1293
1294
1295
1296

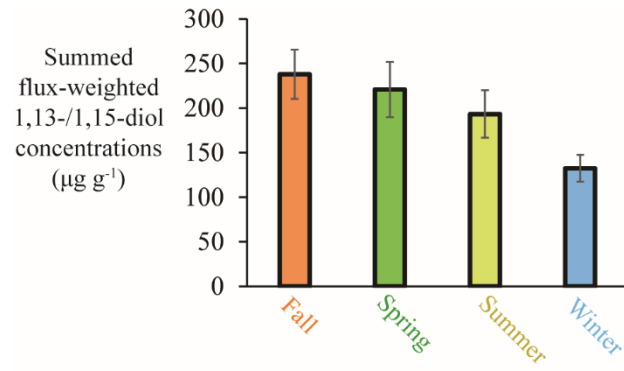
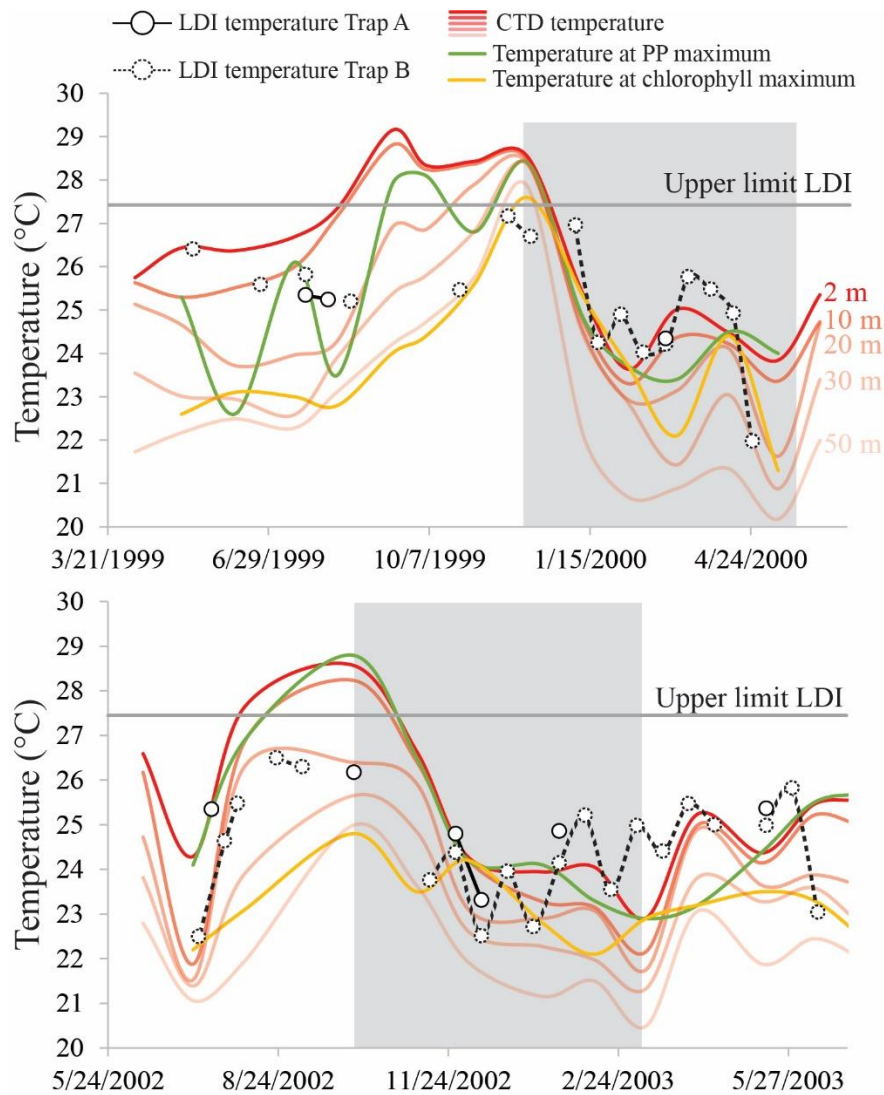


Fig. 4-9 Seasonal summed flux-weighted average of 1,13-/1,15-diol concentrations in all sediment traps (station M1 upper trap, station M2 upper and lower trap and station M4 upper and lower trap) of the tropical North Atlantic.



1297

1298 **Fig. 10** LDI temperature records for the Cariaco Basin time series May 1991 – May 2000 and July 2002
 1299 – July 2003 for Trap A (275 m depth; solid symbols) and Trap B (455 m depth; dashed symbols), with
 1300 CTD-derived temperatures at 2, 10, 20, 30 and 50 m depth (in red;
 1301 <http://www.imars.usf.edu/CAR/index.html>; CARIACO time series composite CTD profiles), the
 1302 temperature at the depth of maximum primary production (green) and the temperature at the depth of
 1303 the chlorophyll maximum (yellow; data adapted from Turich et al., 2013). The shaded area represents
 1304 the upwelling season.

1305

1306